

Antiparticle of exciton in semimetals

Lingxian Kong,¹ Ryuichi Shindou,^{1,*} and Yeyang Zhang^{1,†}

¹International Center for Quantum Materials, School of Physics, Peking University, Beijing 100871, China

(Dated: April 1, 2022)

An emergent quantized field enriches quantum many-body systems. We propose an antiparticle analog of the exciton in semimetals as an emergent collective mode in interacting electron systems. To this end, we solve the Bethe-Salpeter equation of a two-band electron-hole model for semimetals, and demonstrate that inter-band excitations in semimetals are generally comprised of both excitons and antiparticles of excitons. We clarify that the effective theory of the inter-band excitations is given by a generalized Klein-Gordon theory. The particle and antiparticle are characterized by opposite conserved charges, fostering fertile scattering processes as well as possible experimental detections of the antiparticles. Our theory provides a comprehensive understanding of excitonic spectra in generic semimetals, bringing a new insight into electronic collective phenomena in solids.

Introduction—The existence of antiparticles is one of the most striking predictions by the quantum field theory [1]. It renews the basic concept of particles by showing that particle numbers are no longer conserved quantities. In elementary particle physics, every particle has a corresponding antiparticle. Some particles are their own antiparticles, such as photons and Higgs bosons; while others are not, such as electrons and quarks [2]. A pair of particle and antiparticle can be simultaneously created and/or annihilated. A typical example is an annihilation of an electron-positron pair producing two photons.

Electromagnetic and optical properties of solid-state materials are related to emergent collective modes in quantum many-particle systems of electrons and cations. Energy scales of the collective modes are typically much lower than those in high-energy experiments, while effective field theories of the emergent degrees of freedom often share rich mathematical structures with elementary particles in high-energy physics. Thus, it is an important quest to find collective modes in condensed matter systems as analogs of antiparticles.

We demonstrate universal existence of antiparticle analogs of excitons in semimetals, where conduction and valence bands overlap directly or indirectly. In semiconductors, an exciton is a non-relativistic boson that describes a bound state of a conduction-band electron and a valence-band hole. The bound states are eigenstates of a two-body Hamiltonian of the electron and hole that interact through the long-range Coulomb interaction [3–5]. Excitons play crucial roles in optoelectronic properties in semiconductors [6–8]. In semimetals or narrow-gap semiconductors where the conduction and valence bands overlap or nearly overlap, excitons may undergo Bose-Einstein condensation [9–13]. The condensates are described by a Ginzburg-Landau theory as in superconductivity [14–16]. Preceding theories of excitons and their condensates lack the antiparticle analog of excitons. Few theories studied excitonic spectra in semimetals, though the inter-band bound states in the semimetals can be well-defined quasiparticles in certain ranges of the crys-

tal momentum like collective modes in Fermi liquids.

In this Letter, we introduce a concept and realization of antiparticle of the exciton in semimetals by solving the Bethe-Salpeter (BS) equation for a two-band model with screened Coulomb interaction in two and three dimensions (Fig. 1). An inter-band two-particle Green’s function obtained from the BS equation has *two* poles for the $1s$ exciton level ($1s$ hydrogen-atom-type orbital for the relative coordinate between the electron and hole). The inverse of the two-particle Green’s function plays the role of the Lagrangian of free excitons [4]. The Lagrangian takes the form of a generalized Klein-Gordon field theory without the Lorentz symmetry. By quantizing the effective field theory [1], we show that the pair of poles can be interpreted as an exciton and an antiparticle of the exciton (‘antiexciton’), respectively. A calculation of the conserved charge of the effective field theory shows that the exciton and antiexciton can carry opposite physical

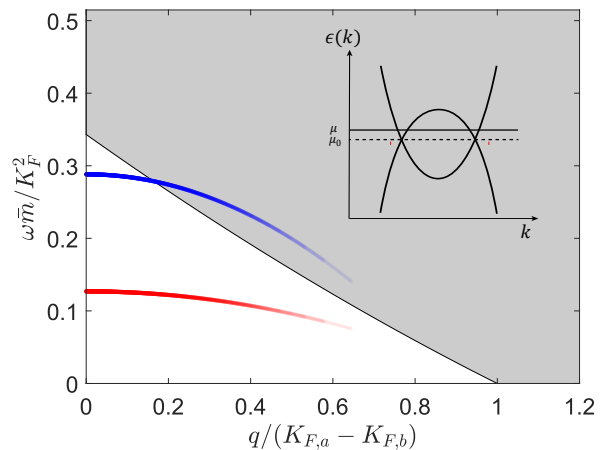


FIG. 1. Energy-momentum (ω - q) dispersions of the s -wave exciton (the red line) and antiexciton (the blue line) bands together with an energy-momentum region of inter-band individual excitations (the shaded region) for a parameter set as in Fig. 2(a). The inset is the kinetic energies of electrons as a function of k .

charges such as spin. The difference can be utilized for distinguishing antiexcitons from excitons experimentally. The opposite charges also enable pair annihilation of excitons and antiexcitons which produces a pair of density waves in conduction and valence bands.

Model—We study a two-band semimetal Hamiltonian with a valence band maximum at $\mathbf{k} = 0$ and a conduction band minimum at $\mathbf{k} = \mathbf{k}_c$ [14, 17]. The kinetic energy part of the electronic Hamiltonian is given by

$$\hat{K}_0 = \sum_{\mathbf{k}} \left[(\epsilon_a(\mathbf{k}) - \mu) a_{\mathbf{k}}^\dagger a_{\mathbf{k}} + (\epsilon_b(\mathbf{k}) - \mu) b_{\mathbf{k}}^\dagger b_{\mathbf{k}} \right] \quad (1)$$

with

$$\epsilon_a(\mathbf{k}) = \frac{k^2}{2m_a} + \frac{E_g}{2}, \quad \epsilon_b(\mathbf{k}) = -\frac{k^2}{2m_b} - \frac{E_g}{2}. \quad (2)$$

Here m_a and m_b are effective masses of a and b bands, respectively. The reduced Planck constant \hbar is set to 1. E_g is an energy difference between the a -band energy minimum and the b -band energy maximum. E_g is negative for the semimetal case. We define $a_{\mathbf{k}}^\dagger$ and $a_{\mathbf{k}}$ as creation and annihilation operators for electrons of the conduction band with wave vector $\mathbf{k} + \mathbf{k}_c$, while $b_{\mathbf{k}}^\dagger$ and $b_{\mathbf{k}}$ for electrons of the valence band with wave vector \mathbf{k} . A charge neutrality (the electron density equals the hole density) can be realized by a chemical potential of $\mu_0 = \frac{E_g(m_a - m_b)}{2(m_a + m_b)}$. To study the inter-band bound states with their crystal momenta \mathbf{q} around \mathbf{k}_c , we put the chemical potential away from the charge neutrality point, $\mu > \mu_0$, where inter-band electron-hole individual excitations have a finite gap at $\mathbf{q} = \mathbf{k}_c$ (for the case of $\mathbf{k}_c = \mathbf{0}$, see Fig. 1). The radii of the Fermi surfaces of a and b bands are denoted as $K_{F,a}$ and $K_{F,b}$ ($K_{F,a} \neq K_{F,b}$). For clarity of presentation, we put $\mathbf{k}_c = \mathbf{0}$ henceforth, while the following argument can be directly applied to the case of $\mathbf{k}_c \neq \mathbf{0}$ [14].

Electrons in the two bands interact through the long-range Coulomb interaction. The interaction takes the following form in the momentum representation,

$$\hat{V} = \frac{1}{2\Omega} \sum_{\mathbf{q}} v(\mathbf{q}) \hat{\rho}(\mathbf{q}) \hat{\rho}(-\mathbf{q}), \quad (3)$$

with a total volume of the system Ω . Here $\hat{\rho}(\mathbf{q})$ stands for the density operator with momentum \mathbf{q} [14, 17],

$$\hat{\rho}(\mathbf{q}) = \sum_{\mathbf{k}} \left(a_{\mathbf{k}+\mathbf{q}}^\dagger a_{\mathbf{k}} + b_{\mathbf{k}+\mathbf{q}}^\dagger b_{\mathbf{k}} \right), \quad (4)$$

and $v(\mathbf{q})$ is the Fourier transform of the bare Coulomb potential given by $v(\mathbf{q}) = \frac{4\pi}{q^2}$ in three dimensions (3D) and $v(\mathbf{q}) = \frac{2\pi}{q}$ in two dimensions (2D). The elementary charge e and the Coulomb constant $(4\pi\epsilon_0)^{-1}$ are set to 1. Since the Hamiltonian, $\hat{K}_0 + \hat{V}$, has no single-particle inter-band hopping terms, the interacting model has a $U(1) \times U(1)$ symmetry.

Inter-band two-particle Green's function—Suppose that a many-body ground state of the interacting electron system does not break the $U(1) \times U(1)$ symmetry. Therefore, it is in the eigenspace of total particle-number operators of a - and b -band electrons, $|N_a, N_b\rangle$, where N_a and N_b denote the electron numbers in a and b bands, respectively. Then, the inter-band excited eigenstates in the semimetals can be either in $|N_a + 1, N_b - 1\rangle$ or in $|N_a - 1, N_b + 1\rangle$. Excitons and antiexcitons are nothing but bound states living in the former and later eigenspace, respectively. To see this, let us use a spectral representation of the zero-temperature time-ordered Green's function for the inter-band excitations, $G^{ex}(\mathbf{x} - \mathbf{x}', t - t')_{\mathbf{y}\mathbf{y}'} = -(-i)^2 \langle \mathcal{T} \{ a_{\mathbf{x}}(t) b_{\mathbf{x}+\mathbf{y}}^\dagger(t) b_{\mathbf{x}'+\mathbf{y}'}(t') a_{\mathbf{x}'}^\dagger(t') \} \rangle$. Here $\langle \dots \rangle$ denotes an expectation value with respect to the many-body ground state, and \mathcal{T} denotes the time-ordered product [18]. In the semimetals, the Fourier transform of $G^{ex}(\mathbf{x} - \mathbf{x}', t - t')_{\mathbf{y}\mathbf{y}'}$, $G^{ex}(\mathbf{q}, \omega)_{\mathbf{k}\mathbf{k}'}$, can be decomposed not only by the excited eigenstates in $|N_a + 1, N_b - 1\rangle$ but also by those in $|N_a - 1, N_b + 1\rangle$ as

$$G^{ex}(\mathbf{q}, \omega)_{\mathbf{k}\mathbf{k}'} = \sum_n \frac{i \langle 0 | b_{\mathbf{k}+\mathbf{q}+\mathbf{k}}^\dagger | n \rangle \langle n | a_{\mathbf{q}+\mathbf{k}}^\dagger b_{\mathbf{k}'} | 0 \rangle}{\omega - (E_n - E_0) + i0^+} - \sum_{n'} \frac{i \langle 0 | a_{\mathbf{q}+\mathbf{k}}^\dagger b_{\mathbf{k}'} | n' \rangle \langle n' | b_{\mathbf{k}}^\dagger a_{\mathbf{q}+\mathbf{k}} | 0 \rangle}{\omega + (E_{n'} - E_0) - i0^+}. \quad (5)$$

Here $|0\rangle$ is the many-body ground state in $|N_a, N_b\rangle$ with the ground-state energy E_0 . \mathbf{q} and ω correspond to the total momentum and frequency of the inter-band bound states, and \mathbf{k}, \mathbf{k}' are relative momenta. $|n\rangle$ and $|n'\rangle$ are the excited eigenstates with the momentum \mathbf{q} and $-\mathbf{q}$ and with the energy E_n and $E_{n'}$ in the eigenspaces of $|N_a + 1, N_b - 1\rangle$ and $|N_a - 1, N_b + 1\rangle$, respectively. Excitons and antiexcitons are bound states comprised of inter-band excitations in $|N_a + 1, N_b - 1\rangle$ and $|N_a - 1, N_b + 1\rangle$, respectively. In the spectral representation, they can be detected as poles in the fourth and second quadrant in the complex- ω plane, respectively. In a semiconductor with $E_g > 0$ and $N_a = 0$, the inter-band excited eigenstates are only in the space of $|N_a + 1, N_b - 1\rangle$. Thus, there is no antiparticle-type exciton in the semiconductor regime. Note also that pair annihilation of excitons and antiexcitons in the semimetals leads to an excited state in $|N_a, N_b\rangle$, which comprises of an intraband particle-hole excitation in the a band and that in the b band (see below).

The inter-band two-particles Green's function can be legitimately calculated by the screened-ladder approximation in the dilute carrier-density limit [4, 18–20]. Under this approximation with a proper normalization $\tilde{G}^{ex}(\mathbf{q}, \omega)_{\mathbf{k}\mathbf{k}'} \equiv -iG^{ex}(\mathbf{q}, \omega)_{\mathbf{k}\mathbf{k}'}/\Omega$, the Fourier transform is given by a solution of the matrix-form BS equation [4, 19, 21],

$$\tilde{G}^{ex}(\mathbf{q}, \omega) = \tilde{G}_0^{ex}(\mathbf{q}, \omega) - \tilde{G}_0^{ex}(\mathbf{q}, \omega) W \tilde{G}^{ex}(\mathbf{q}, \omega), \quad (6)$$

or

$$\tilde{G}^{ex}(\mathbf{q}, \omega)^{-1} = \tilde{G}_0^{ex}(\mathbf{q}, \omega)^{-1} + W. \quad (7)$$

$G_0^{ex}(\mathbf{q}, \omega)_{\mathbf{k}\mathbf{k}'}$ $\equiv i\Omega\tilde{G}_0^{ex}(\mathbf{q}, \omega)_{\mathbf{k}\mathbf{k}'}$ is the Fourier transform of the non-interacting two-particle Green's function and $w(\mathbf{k} - \mathbf{k}') \equiv \Omega W_{\mathbf{k}\mathbf{k}'}$ is the Fourier transform of the static screened Coulomb potential. In the random phase approximation (RPA) [22], the screened Coulomb potential is given by the Thomas-Fermi (TF) wavelength k_{TF} as $w(\mathbf{k}) = 4\pi/(k^2 + k_{\text{TF}}^2)$ in 3D and $w(\mathbf{k}) = 2\pi/(k + k_{\text{TF}})$ in 2D. The TF wavevector is calculated as $k_{\text{TF}}^2 = 2(K_{F,a}m_a + K_{F,b}m_b)/\pi$ in 3D and $k_{\text{TF}} = m_a + m_b$ in 2D. By solving the eigenvalue problem $\tilde{G}^{ex}(\mathbf{q}, \omega)^{-1}|\phi_j(\mathbf{q}, \omega)\rangle = \xi_j(\mathbf{q}, \omega)|\phi_j(\mathbf{q}, \omega)\rangle$ and $\xi_j(\mathbf{q}, \omega) = 0$, we obtain eigenenergies ($\omega = E_n - E_0$ or $-\omega = E_{n'} - E_0$) and eigen-wavefunctions for the inter-band bound states in the semimetals.

Inter-band bound states at the Γ point—We focus on the solutions at $\mathbf{q} = 0$. Thereby, $G^{ex}(\mathbf{0}, \omega)$ has the spatially rotational symmetry, i.e. $G^{ex}(\mathbf{0}, \omega)_{\mathbf{k}\mathbf{k}'} = G^{ex}(\mathbf{0}, \omega)_{\tilde{\mathbf{k}}\tilde{\mathbf{k}'}}$, where $\tilde{\mathbf{k}}$ and $\tilde{\mathbf{k}'}$ are transformed into \mathbf{k} and \mathbf{k}' respectively by the same rotation. The eigenvalue problem at the Γ point is decomposed by the irreducible representations of the rotational symmetry group [20]. The Green's function is expanded by spherical harmonics in the 3D case,

$$-iG^{ex}(\mathbf{0}, \omega)_{\mathbf{k}\mathbf{k}'} = \sum_{nlm} \frac{Y_{lm}(\theta, \varphi) f_{nl}(\omega; k) f_{nl}(\omega; k') Y_{lm}^*(\theta', \varphi')}{\xi_{nl}(\omega)} \quad (8)$$

and by trigonometric functions in the 2D case,

$$-iG^{ex}(\mathbf{0}, \omega)_{\mathbf{k}\mathbf{k}'} = \sum_{nm} \frac{f_{nm}(\omega; k) f_{nm}(\omega; k') e^{im(\varphi - \varphi')}}{\xi_{nm}(\omega)}. \quad (9)$$

Here $\mathbf{k} = k(\sin\theta \cos\varphi, \sin\theta \sin\varphi, \cos\theta)$ in the 3D case and $\mathbf{k} = k(\cos\varphi, \sin\varphi)$ in the 2D case. $f_{nl}(\omega; k)$ and $f_{nm}(\omega; k)$ stand for radial wavefunctions and $Y_{lm}(\theta, \varphi)$ are the spherical harmonics. In the 3D and 2D case, $\langle \mathbf{k} | \phi_j(\mathbf{0}, \omega) \rangle = \frac{1}{\sqrt{\Omega}} f_{nl}(\omega; k) Y_{lm}(\theta, \varphi)$ and $\langle \mathbf{k} | \phi_j(\mathbf{0}, \omega) \rangle = \frac{1}{\sqrt{\Omega}} f_{nm}(\omega; k) e^{im\varphi}$ where j is the combination of principal quantum number n , azimuthal quantum number l in the 3D case, and magnetic quantum number m . Fig. 2 plots $\xi_j(\mathbf{0}, \omega)$ as a function of ω . Individual inter-band excitations with $\mathbf{q} = 0$ form continuum spectra in certain ranges of ω , which correspond to the shaded regions in the figure. Apart from the continuum spectra, a branch of s -wave ($l = 0$) bound states in 3D and a branch of $m = 0$ bound states in 2D form a parabolic curve of ω outside the shaded region (Fig. 2). The branch crosses zero at both a positive ω ($\omega = \omega_+$) and a negative ω ($\omega = -\omega_-$). The spectral representation dictates that the positive zero corresponds to a bound state in

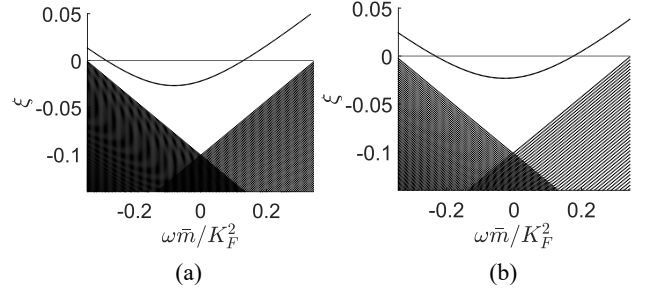


FIG. 2. $\xi_j(\mathbf{q} = \mathbf{0}, \omega)$ as a function of ω , with $m_a = m_b \equiv \tilde{m}$, $K_F \equiv (K_{F,a} + K_{F,b})/2$. Locations of the zeros ($\xi_j(\mathbf{q} = \mathbf{0}, \omega) = 0$) are determined by three dimensionless quantities, $K_F\alpha_B$, $\tilde{E}_g \equiv E_g\tilde{m}/K_F^2$ and $\tilde{\mu} \equiv \mu\tilde{m}/K_F^2$, where the effective Bohr radius $\alpha_B = 1/\tilde{m}$. The electron rest mass m_e is set to 1. (a) 3D case: eigenvalues with $l = 0, m = 0$ are plotted for $K_F\alpha_B = K_F/3.5 = 0.289$, $\tilde{E}_g = -0.3\tilde{m}/K_F^2 = -1.03$, and $\tilde{\mu} = 0.05\tilde{m}/K_F^2 = 0.172$. (b) 2D case: eigenvalues with $m = 0$ are plotted for $K_F\alpha_B = K_F = 0.540$, $\tilde{E}_g = -0.3\tilde{m}/K_F^2 = -1.03$, and $\tilde{\mu} = 0.05\tilde{m}/K_F^2 = 0.172$.

$|N_a + 1, N_b - 1\rangle$ (exciton) and the negative zero corresponds to a bound state in $|N_a - 1, N_b + 1\rangle$ (antiexciton). In fact, this is consistent with a derivative of $\xi_j(\mathbf{0}, \omega)$ with respect to ω at these zeros. In terms of the Feynman-Hellmann theorem [20, 23], one can relate the derivative with the momentum-space wavefunctions,

$$\partial_\omega \xi_j = \sum_{|\mathbf{k}| > K_{\text{out}}} |\langle \mathbf{k} | \phi_j \rangle|^2 - \sum_{|\mathbf{k}| < K_{\text{in}}} |\langle \mathbf{k} | \phi_j \rangle|^2, \quad (10)$$

with $K_{\text{out}} \equiv K_{F,a}$ and $K_{\text{in}} \equiv K_{F,b} (< K_{F,a})$. The relation together with Fig. 2 dictates that the eigenvectors of the positive- ω (negative- ω) bound state has larger spectral weight in $|\mathbf{k}| > K_{\text{out}}$ ($|\mathbf{k}| < K_{\text{in}}$), suggesting that the former and latter bound states are of $a_{\mathbf{k}}^\dagger b_{\mathbf{k}}|0\rangle$ type and of $b_{\mathbf{k}}^\dagger a_{\mathbf{k}}|0\rangle$ type, respectively.

Effective field interpretation— $\xi_j(\mathbf{0}, \omega)$ is an eigenvalue of the inverse of the inter-band two-particle Green's function $\tilde{G}^{ex}(\mathbf{0}, \omega)^{-1}$. To the quadratic level in ω , it can be regarded as an effective Lagrangian for inter-band collective modes at $\mathbf{q} = 0$. Unlike in the semiconductor case, the ω -dependent part of the $\tilde{G}^{ex}(\mathbf{0}, \omega)^{-1}$ matrix in the semimetal case is not simply proportional to an identity matrix. Namely, both of the two terms in the right hand side of Eq. (5) do not vanish in the semimetal case. Thus, $\xi_j(\mathbf{0}, \omega)$ becomes a nonlinear function of ω . The simplest effective Lagrangian for the inter-band collective excitations in semimetals contains an ω^2 term in addition to an ω term, i.e. $\xi_j(\mathbf{0}, \omega) = \gamma\omega^2 + \alpha\omega - \beta$ with $\gamma > 0$ and $\beta > 0$ (see Fig. 2). Thus, the effective Lagrangian contains a second-order time derivative of a complex scalar field φ for the $\mathbf{q} = 0$ inter-band collective modes,

$$\int dt \mathcal{L} = \int dt \varphi^\dagger(t) (-\gamma\partial_t^2 + i\alpha\partial_t - \beta)\varphi(t). \quad (11)$$

The complex field is decomposed into two real fields, φ_1 and φ_2 , as $\varphi \equiv \varphi_1 + i\varphi_2$. Two conjugate momenta are introduced as $\pi_1 \equiv \frac{\partial \mathcal{L}}{\partial(\partial_t \varphi_1)}$ and $\pi_2 \equiv \frac{\partial \mathcal{L}}{\partial(\partial_t \varphi_2)}$. This leads to an effective Hamiltonian for the inter-band collective modes in semimetals as:

$$\begin{aligned} \mathcal{H} &= \pi_1 \partial_t \varphi_1 + \pi_2 \partial_t \varphi_2 - \mathcal{L} \\ &= \frac{1}{2\lambda} (\pi_1^2 + \pi_2^2) + \frac{1}{2} \lambda \eta^2 (\varphi_1^2 + \varphi_2^2) + \frac{\alpha}{2\gamma} (\pi_2 \varphi_1 - \pi_1 \varphi_2). \end{aligned} \quad (12)$$

Here $\lambda = 2\gamma$, and $\eta = \sqrt{\frac{\alpha^2}{4\gamma^2} + \frac{\beta}{\gamma}}$. The Hamiltonian takes a form of two coupled harmonic oscillators and is bosonized by two boson fields:

$$\mathcal{H} = \nu_+ a_+^\dagger a_+ + \nu_- a_-^\dagger a_-, \quad (13)$$

with

$$a_{1,2} \equiv \sqrt{\frac{\lambda \eta}{2}} \left(\varphi_{1,2} + \frac{i}{\lambda \eta} \pi_{1,2} \right), \quad a_{\pm} \equiv \frac{1}{\sqrt{2}} (a_1 \pm i a_2), \quad (14)$$

and

$$\nu_{\pm} = \sqrt{\frac{\alpha^2}{4\gamma^2} + \frac{\beta}{\gamma}} \mp \frac{\alpha}{2\gamma}. \quad (15)$$

Note that within the quadratic expansion of $\xi_j(\mathbf{0}, \omega)$ in ω , the two zeros of $\xi_j(\mathbf{0}, \omega)$ correspond to the quantized energies of the two bosons, $\nu_{\pm} = \omega_{\pm} (> 0)$. This concludes that a_+ and a_- boson operators represent the exciton and antiexciton annihilation operators, respectively. When $\alpha \neq 0$, the Hamiltonian describes two non-degenerate harmonic oscillators, whereas the Klein-Gordon theory (the $\alpha = 0$ case) describes two degenerate harmonic oscillators [1]. Thus, we can view the inter-band collective modes in semimetals as a “CP-violated” Klein-Gordon field without the Lorentz symmetry.

Conserved charge—The Lagrangian in Eq. (11) is invariant under a U(1) transformation $\varphi \rightarrow \varphi e^{i\theta}$. By Noether’s theorem, it has a conserved charge density [1, 21]:

$$j^0 = -i\varphi \frac{\partial \mathcal{L}}{\partial(\partial_t \varphi)} + i\varphi^\dagger \frac{\partial \mathcal{L}}{\partial(\partial_t \varphi^\dagger)}. \quad (16)$$

A calculation shows that an exciton and an antiexciton carry opposite values of the conserved charge [20],

$$j^0 = a_+^\dagger a_+ - a_-^\dagger a_-. \quad (17)$$

When the a -band and b -band electrons have an opposite physical property such as spin, the conserved charge carries the physical property. This is because a joint U(1) transformation, $a_{\mathbf{k}} \rightarrow a_{\mathbf{k}} e^{i\frac{\theta}{2}}$ and $b_{\mathbf{k}} \rightarrow b_{\mathbf{k}} e^{-i\frac{\theta}{2}}$, leads to $\varphi \rightarrow \varphi e^{i\theta}$ with $\varphi \propto b^\dagger a$. Suppose that the a -band

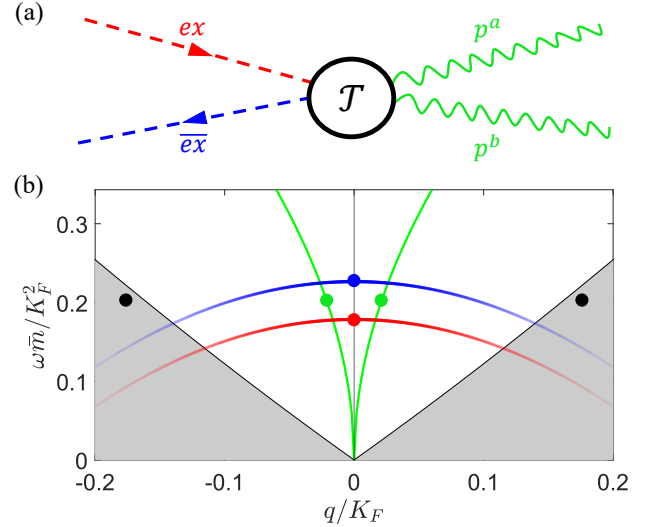


FIG. 3. (a) An annihilation process of an exciton-antiexciton pair. ex and \bar{ex} stand for an exciton and an antiexciton, while p^a and p^b represent intra-band particle-hole excitation in the a and b band, respectively. (b) Dispersions of the s -wave exciton (red) and antiexciton (blue) bands, plasmon band (green) and intra-band individual excitations (the grey shaded area) around the Γ point in the 2D case for the same parameters as Fig. 2 (b). The pair annihilation of $\mathbf{q} = 0$ exciton and antiexciton (the red and blue points) leads to two intra-band particle-hole excitations, which can be either individual excitations (the black points) or plasmons (the green points).

electrons are with spin-up polarization along z -direction, and the b -band electrons are with spin-down polarization. Then exciton states carry $S_z = 1$ and antiexciton states carry $S_z = -1$. This can be also seen from the spectral representation of the Green’s function, Eq. (5). In this case, spin-polarized excitation spectroscopy could distinguish exciton states from antiexciton states experimentally [24, 25].

Band curvatures around the Γ point—Energies of excitons and antiexcitons at finite \mathbf{q} can be expanded as $\omega_{\pm}(\mathbf{q}) = \omega_{\pm} + q^2/(2M)$ to the lowest order in q . The band curvature $1/(2M)$ can be calculated from the irreducible representations of Eq. (7). In parameter ranges studied in this paper, the band curvatures always take negative values both for the exciton and antiexciton bands [20]. When energies of these inter-band bound states touch zero at finite \mathbf{q} , the system can undergo Bose-Einstein condensation. When the exciton or antiexciton condensates, the two bound-state modes become a Goldstone mode and a Higgs mode [26–29].

Exciton-antiexciton pair annihilation—As excited eigenstates, an exciton or an antiexciton around $\mathbf{q} = 0$ does not decay into inter-band individual excitations by themselves. Nonetheless, a pair of the exciton and the antiexciton can decay into multiple intra-band individual excitations or collective modes [18, 30]. For example, in the eigenspace of $|N_a, N_b\rangle$, the energy-momentum

conservation allows the pair to decay into two intra-band excitations (Fig. 3).

Summary and Discussion—In this Letter, we demonstrate the universal existence of the antiparticle analog of the exciton (‘antiexciton’) in semimetals. Our theory is relevant to inter-band excitation spectra in semimetal materials, such as As, Sb, and HgTe. It is also relevant to electron-hole double-layer systems such as semiconductor heterostructures and bilayer 2D materials [31–38]. Optical absorption and photoluminescence can be experimental probes of the antiparticle analog of the exciton in these materials [39–42].

We thank Zhenyu Xiao, Weiliang Qiao, and Qingzheng Qiu for helpful discussions. The work was supported by the National Basic Research Programs of China (No. 2019YFA0308401) and by National Natural Science Foundation of China (No. 11674011 and No. 12074008).

* Corresponding author. rshindou@pku.edu.cn

† Corresponding author. yeyzhang@pku.edu.cn

- [1] M. Srednicki, *Quantum Field Theory* (Cambridge University Press, 2007).
- [2] D. Griffiths, *Introduction to elementary particles* (John Wiley & Sons, 2020).
- [3] M. Rohlfing and S. G. Louie, Electron-hole excitations and optical spectra from first principles, *Phys. Rev. B* **62**, 4927 (2000).
- [4] R. M. Martin, L. Reining, and D. M. Ceperley, *Interacting Electrons: Theory and Computational Approaches* (Cambridge University Press, 2016).
- [5] G. Strinati, Application of the Green’s functions method to the study of the optical properties of semiconductors, *La Rivista del Nuovo Cimento* (1978-1999) **11**, 1 (1988).
- [6] S. Koch, M. Kira, G. Khitrova, and H. Gibbs, Semiconductor excitons in new light, *Nature materials* **5**, 523 (2006).
- [7] R. A. Kaindl, M. A. Carnahan, D. Hägele, R. Löwenich, and D. S. Chemla, Ultrafast terahertz probes of transient conducting and insulating phases in an electron-hole gas, *Nature* **423**, 734 (2003).
- [8] M. Kira, F. Jahnke, and S. W. Koch, Microscopic theory of excitonic signatures in semiconductor photoluminescence, *Phys. Rev. Lett.* **81**, 3263 (1998).
- [9] B. Halperin and T. Rice, The excitonic state at the semiconductor-semimetal transition, in *Solid State Physics*, Vol. 21 (Elsevier, 1968) pp. 115–192.
- [10] B. I. Halperin and T. M. Rice, Possible anomalies at a semimetal-semiconductor transition, *Rev. Mod. Phys.* **40**, 755 (1968).
- [11] A. Kozlov and L. Maksimov, The metal-dielectric divalent crystal phase transition, *Sov. Phys. JETP* **21**, 790 (1965).
- [12] E. Hanamura and H. Haug, Condensation effects of excitons, *Physics Reports* **33**, 209 (1977).
- [13] A. Kogar, M. S. Rak, S. Vig, A. A. Husain, F. Flicker, Y. I. Joe, L. Venema, G. J. MacDougall, T. C. Chiang, E. Fradkin, J. van Wezel, and P. Abbamonte, Signatures of exciton condensation in a transition metal dichalcogenide, *Science* **358**, 1314 (2017).
- [14] D. Jérôme, T. M. Rice, and W. Kohn, Excitonic insulator, *Phys. Rev.* **158**, 462 (1967).
- [15] J. M. Blatt, K. W. Böer, and W. Brandt, Bose-Einstein condensation of excitons, *Phys. Rev.* **126**, 1691 (1962).
- [16] P. B. Littlewood, P. R. Eastham, J. M. J. Keeling, F. M. Marchetti, B. D. Simons, and M. H. Szymanska, Models of coherent exciton condensation, *Journal of Physics: Condensed Matter* **16**, S3597 (2004).
- [17] J. D. Cloizeaux, Exciton instability and crystallographic anomalies in semiconductors, *Journal of Physics and Chemistry of Solids* **26**, 259 (1965).
- [18] A. L. Fetter and J. D. Walecka, *Quantum theory of many-particle systems* (Courier Corporation, 2012).
- [19] A. Marini and R. Del Sole, Dynamical excitonic effects in metals and semiconductors, *Phys. Rev. Lett.* **91**, 176402 (2003).
- [20] See Supplemental Material at [url will be inserted by publisher] for derivation of the Bethe-Salpeter equation and its irreducible representations at the Γ point, solutions of band energies and band curvatures around the Γ point, discussions about the exciton-antiexciton pair annihilation, and conserved-charge analyses of the effective field theory.
- [21] A. Altland and B. D. Simons, *Condensed Matter Field Theory*, 2nd ed. (Cambridge University Press, 2010).
- [22] B. Mihaila, Lindhard function of a d-dimensional Fermi gas, [arXiv:1111.5337](https://arxiv.org/abs/1111.5337).
- [23] D. J. Griffiths and D. F. Schroeter, *Introduction to Quantum Mechanics*, 3rd ed. (Cambridge University Press, 2018).
- [24] M. Maialle and L. Sham, Exciton spin dynamics and polarized luminescence in quantum wells, *Surface Science* **305**, 256 (1994).
- [25] X.-X. Zhang, Y. You, S. Y. F. Zhao, and T. F. Heinz, Experimental evidence for dark excitons in monolayer WSe₂, *Phys. Rev. Lett.* **115**, 257403 (2015).
- [26] D. Pekker and C. Varma, Amplitude/Higgs modes in condensed matter physics, *Annual Review of Condensed Matter Physics* **6**, 269 (2015).
- [27] P. B. Littlewood and C. M. Varma, Gauge-invariant theory of the dynamical interaction of charge density waves and superconductivity, *Phys. Rev. Lett.* **47**, 811 (1981).
- [28] P. B. Littlewood and C. M. Varma, Amplitude collective modes in superconductors and their coupling to charge-density waves, *Phys. Rev. B* **26**, 4883 (1982).
- [29] C. Varma, Higgs boson in superconductors, *Journal of low temperature physics* **126**, 901 (2002).
- [30] G. Giuliani and G. Vignale, *Quantum Theory of the Electron Liquid* (Cambridge University Press, 2005).
- [31] A. Jain, S. P. Ong, G. Hautier, W. Chen, W. D. Richards, S. Dacek, S. Cholia, D. Gunter, D. Skinner, G. Ceder, and K. a. Persson, The Materials Project: A materials genome approach to accelerating materials innovation, *APL Materials* **1**, 011002 (2013).
- [32] X. Wu, W. Lou, K. Chang, G. Sullivan, and R.-R. Du, Resistive signature of excitonic coupling in an electron-hole double layer with a middle barrier, *Phys. Rev. B* **99**, 085307 (2019).
- [33] Y. Jiang, S. Thapa, G. D. Sanders, C. J. Stanton, Q. Zhang, J. Kono, W. K. Lou, K. Chang, S. D. Hawkins, J. F. Klem, W. Pan, D. Smirnov, and Z. Jiang, Probing the semiconductor to semimetal transition in InAs/GaSb

- double quantum wells by magneto-infrared spectroscopy, *Phys. Rev. B* **95**, 045116 (2017).
- [34] L. Du, X. Li, W. Lou, G. Sullivan, K. Chang, J. Kono, and R.-R. Du, Evidence for a topological excitonic insulator in InAs/GaSb bilayers, *Nature communications* **8**, 1 (2017).
- [35] J. Li, T. Taniguchi, K. Watanabe, J. Hone, and C. Dean, Excitonic superfluid phase in double bilayer graphene, *Nature Physics* **13**, 751 (2017).
- [36] K. Chen and R. Shindou, Helicoidal excitonic phase in an electron-hole double-layer system, *Phys. Rev. B* **100**, 035130 (2019).
- [37] Y. Zhang and R. Shindou, Dissipationless spin-charge conversion in excitonic pseudospin superfluid, *Phys. Rev. Lett.* **128**, 066601 (2022).
- [38] H. Kroemer, The 6.1 a family (InAs, GaSb, AlSb) and its heterostructures: a selective review, *Physica E: Low-dimensional Systems and Nanostructures* **20**, 196 (2004).
- [39] W. Y. Liang, Excitons, *Physics Education* **5**, 226 (1970).
- [40] M. Kira, F. Jahnke, and S. W. Koch, Quantum theory of secondary emission in optically excited semiconductor quantum wells, *Phys. Rev. Lett.* **82**, 3544 (1999).
- [41] B. Brar, H. Kroemer, J. Ibbetson, and J. H. English, Photoluminescence from narrow InAs-AlSb quantum wells, *Applied Physics Letters* **62**, 3303 (1993).
- [42] Y. Wakisaka, T. Sudayama, K. Takubo, T. Mizokawa, M. Arita, H. Namatame, M. Taniguchi, N. Katayama, M. Nohara, and H. Takagi, Excitonic insulator state in Ta₂NiSe₅ probed by photoemission spectroscopy, *Phys. Rev. Lett.* **103**, 026402 (2009).

SUPPLEMENTARY MATERIAL FOR “ANTIPARTICLE OF EXCITON IN SEMIMETALS”

In this supplementary material, we use the Hartree atomic units to take the reduced Planck constant \hbar , the elementary charge e , the electron rest mass m_e , and the Coulomb constant $(4\pi\epsilon_0)^{-1}$ to be 1.

Bethe-Salpeter equation for the two-particle function and derivation of Eq. (10) in the main text

This section provides a detailed derivation of Eqs. (6,7) and Eq. (10) together with a screened Coulomb interaction $w(\mathbf{q})$ in two dimensions (2D) and three dimensions (3D). Define a time-ordered inter-band two-particle Green's function in the zero-temperature ($T = 0$) field theory:

$$G^{ex}(\mathbf{x} - \mathbf{x}', t - t')_{\mathbf{y}\mathbf{y}'} = -(-i)^2 \langle 0 | \mathcal{T} \{ a_{\mathbf{x}}(t) b_{\mathbf{x}+\mathbf{y}}^\dagger(t) b_{\mathbf{x}'+\mathbf{y}'}(t') a_{\mathbf{x}'}^\dagger(t') \} | 0 \rangle. \quad (\text{S.1})$$

Here $|0\rangle$ denotes a many-body ground state in the $|N_a, N_b\rangle$ Hilbert space where N_a and N_b are electron numbers in a and b bands. $a_{\mathbf{x}}$ and $b_{\mathbf{x}}$ are annihilation operators in the a and b bands. $a_{\mathbf{k}}$ and $b_{\mathbf{k}}$ in Eq. (1) in the main text are Fourier transforms of $a_{\mathbf{x}}$ and $b_{\mathbf{x}}$, e.g.

$$a_{\mathbf{x}} = \frac{1}{\sqrt{\Omega}} \sum_{\mathbf{k}} e^{i\mathbf{k}\mathbf{x}} a_{\mathbf{k}}, \quad b_{\mathbf{x}} = \frac{1}{\sqrt{\Omega}} \sum_{\mathbf{k}} e^{i\mathbf{k}\mathbf{x}} b_{\mathbf{k}}. \quad (\text{S.2})$$

with a total volume of the system Ω . \mathbf{y} and \mathbf{y}' in Eq. (S.1) are relative distances between the particle and hole that form a bound state. $\mathbf{x} + \frac{m_b}{m_a+m_b}\mathbf{y}$, $\mathbf{x}' + \frac{m_b}{m_a+m_b}\mathbf{y}'$ can be regarded as the center-of-mass coordinates of the particle and hole.

In the dilute limit of the carrier densities, the two-particle Green's function can be evaluated in terms of the ladder approximation represented by the Feynman diagram Fig. S.1 [18],

$$G^{ex}(\mathbf{x} - \mathbf{x}', t - t')_{\mathbf{y}\mathbf{y}'} = G_0^{ex}(\mathbf{x} - \mathbf{x}', t - t')_{\mathbf{y}\mathbf{y}'} + i \int d^d\bar{\mathbf{x}} \int d^d\bar{\mathbf{y}} \int d\bar{t} \quad G_0^{ex}(\mathbf{x} - \bar{\mathbf{x}}, t - \bar{t})_{\mathbf{y}\bar{\mathbf{y}}} w(\bar{\mathbf{y}}) G^{ex}(\bar{\mathbf{x}} - \mathbf{x}', \bar{t} - t')_{\bar{\mathbf{y}}\mathbf{y}'}, \quad (\text{S.3})$$

where $G_0^{ex}(\mathbf{x} - \mathbf{x}', t - t')_{\mathbf{y}\mathbf{y}'}$ denotes the two-particle Green's function in a free theory ($V = 0$),

$$G_0^{ex}(\mathbf{x} - \mathbf{x}', t - t')_{\mathbf{y}\mathbf{y}'} = G_0^a(\mathbf{x} - \mathbf{x}', t - t') G_0^b(\mathbf{x}' - \mathbf{x} + \mathbf{y}' - \mathbf{y}, t' - t). \quad (\text{S.4})$$

Here G_0^a and G_0^b are single-particle Green's functions of the a and b bands in the free theory, respectively,

$$\begin{aligned} iG_0^a(\mathbf{x} - \mathbf{x}', t - t') &= \langle 0 | \mathcal{T} \{ a_{\mathbf{x}}(t) a_{\mathbf{x}'}^\dagger(t') \} | 0 \rangle_{|V=0} \\ &= \Omega^{-1} \sum_{\mathbf{k}} e^{i\mathbf{k}(\mathbf{x}-\mathbf{x}') - i\epsilon_a(\mathbf{k})(t-t')} [\theta(t-t')\theta(|\mathbf{k}| - K_{F,a}) - \theta(t'-t)\theta(K_{F,a} - |\mathbf{k}|)], \end{aligned} \quad (\text{S.5})$$

$$\begin{aligned} iG_0^b(\mathbf{x} - \mathbf{x}', t - t') &= \langle 0 | \mathcal{T} \{ b_{\mathbf{x}}(t) b_{\mathbf{x}'}^\dagger(t') \} | 0 \rangle_{|V=0} \\ &= \Omega^{-1} \sum_{\mathbf{k}} e^{i\mathbf{k}(\mathbf{x}-\mathbf{x}') - i\epsilon_b(\mathbf{k})(t-t')} [\theta(t-t')\theta(K_{F,b} - |\mathbf{k}|) - \theta(t'-t)\theta(|\mathbf{k}| - K_{F,b})]. \end{aligned} \quad (\text{S.6})$$

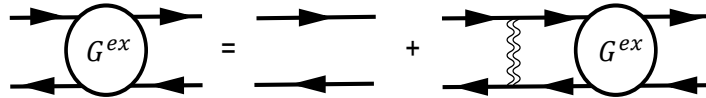


FIG. S.1. The Feynman diagram of the screened-ladder approximation for G^{ex} . The upper and lower solid lines with rightward and leftward arrows are electron propagators in the a band and b band, respectively. The double-wavy line is the screened Coulomb interaction $w(\mathbf{y})$ or $w(\mathbf{k} - \mathbf{k}')$ represented by the Feynman diagram Fig. S.2.

The ground state in the free theory is characterized by a Fermi momentum of the conduction-band Fermi surface, $K_{F,a}$, and Fermi momentum of the valence-band Fermi surface, $K_{F,b}$. Their Fourier transforms are as follows,

$$G_0^a(\mathbf{k}, \omega) = \frac{\theta(|\mathbf{k}| - K_{F,a})}{\omega - \epsilon_a(\mathbf{k}) + i0^+} + \frac{\theta(K_{F,a} - |\mathbf{k}|)}{\omega - \epsilon_a(\mathbf{k}) - i0^+}, \quad G_0^b(\mathbf{k}, \omega) = \frac{\theta(K_{F,b} - |\mathbf{k}|)}{\omega - \epsilon_b(\mathbf{k}) + i0^+} + \frac{\theta(|\mathbf{k}| - K_{F,b})}{\omega - \epsilon_b(\mathbf{k}) - i0^+}. \quad (\text{S.7})$$

In the momentum-frequency space, Eq. (S.3) takes a form of

$$\tilde{G}^{ex}(\mathbf{q}, \omega)_{\mathbf{k}\mathbf{k}'} = \tilde{G}_0^{ex}(\mathbf{q}, \omega)_{\mathbf{k}\mathbf{k}'} - \frac{1}{\Omega} \sum_{\mathbf{k}_1 \mathbf{k}_2} \tilde{G}_0^{ex}(\mathbf{q}, \omega)_{\mathbf{k}\mathbf{k}_1} w(\mathbf{k}_1 - \mathbf{k}_2) \tilde{G}^{ex}(\mathbf{q}, \omega)_{\mathbf{k}_2 \mathbf{k}'}, \quad (\text{S.8})$$

with $i\Omega \tilde{G}^{ex}(\mathbf{q}, \omega)_{\mathbf{k}\mathbf{k}'} \equiv G^{ex}(\mathbf{q}, \omega)_{\mathbf{k}\mathbf{k}'}$ and

$$G^{ex}(\mathbf{q}, \omega)_{\mathbf{k}\mathbf{k}'} = \int d(t-t') \int d^d(\mathbf{x} - \mathbf{x}') \int d^d \mathbf{y} \int d^d \mathbf{y}' e^{i\omega(t-t') - i\mathbf{q} \cdot (\mathbf{x} - \mathbf{x}') + i\mathbf{k} \cdot \mathbf{y} - i\mathbf{k}' \cdot \mathbf{y}'} G^{ex}(\mathbf{x} - \mathbf{x}', t - t')_{\mathbf{y}\mathbf{y}'}. \quad (\text{S.9})$$

The Fourier transform of the free two-particle Green's function is given by

$$\begin{aligned} \tilde{G}_0^{ex}(\mathbf{q}, \omega)_{\mathbf{k}\mathbf{k}'} &= -i\delta_{\mathbf{k}\mathbf{k}'} \int \frac{d\omega_1}{2\pi} G_0^a(\mathbf{k} + \mathbf{q}, \omega_1 + \omega) G_0^b(\mathbf{k}, \omega_1) \\ &= \delta_{\mathbf{k}\mathbf{k}'} \left\{ \frac{\theta(|\mathbf{k} + \mathbf{q}| - K_{F,a})\theta(|\mathbf{k}| - K_{F,b})}{\omega - [\epsilon_a(\mathbf{k} + \mathbf{q}) - \epsilon_b(\mathbf{k})] + i0^+} - \frac{\theta(K_{F,a} - |\mathbf{k} + \mathbf{q}|)\theta(K_{F,b} - |\mathbf{k}|)}{\omega - [\epsilon_a(\mathbf{k} + \mathbf{q}) - \epsilon_b(\mathbf{k})] - i0^+} \right\}. \end{aligned} \quad (\text{S.10})$$

With $W_{\mathbf{k}\mathbf{k}'} \equiv \Omega^{-1} w(\mathbf{k} - \mathbf{k}')$, Eq. (S.8) can be written into a following matrix form [4]

$$\tilde{G}^{ex}(\mathbf{q}, \omega)^{-1} = \tilde{G}_0^{ex}(\mathbf{q}, \omega)^{-1} + W. \quad (\text{S.11})$$

$w(\mathbf{y})$ in Eq. (S.3) stands for an effective interaction between the electron and hole. In a semiconductor regime ($E_g > 0$), it is the long-ranged Coulomb interaction. In a semimetal regime ($E_g < 0$), the Coulomb interaction is screened by carrier densities. The screened Coulomb interaction can be evaluated by the random phase approximation (Fig. S.2). In the approximation, the Fourier transform of $w(\mathbf{y})$ is given by a static limit of the bare polarization function $\Pi_0(\mathbf{q}, \omega)$,

$$w(\mathbf{q}) = \frac{v(\mathbf{q})}{1 - v(\mathbf{q})\Pi_0(\mathbf{0}, 0)} = \begin{cases} \frac{4\pi}{q^2 - 4\pi\Pi_0(\mathbf{0}, 0)}, & \text{in 3D,} \\ \frac{2\pi}{q - 2\pi\Pi_0(\mathbf{0}, 0)}, & \text{in 2D.} \end{cases} \quad (\text{S.12})$$

The bare polarization function in our two-band model is given by

$$\begin{aligned} \Pi_0(\mathbf{q}, \omega) &= \sum_{c=a,b} \Pi_0^c(\mathbf{q}, \omega), \\ \Pi_0^c(\mathbf{q}, \omega) &= -i \int \frac{d\omega_1}{2\pi} \int \frac{d^d \mathbf{k}}{(2\pi)^d} G_0^c(\mathbf{k} + \mathbf{q}, \omega_1 + \omega) G_0^c(\mathbf{k}, \omega_1). \end{aligned} \quad (\text{S.13})$$

The static limit of the polarization function is given by

$$\Pi_0(\mathbf{0}, 0) \equiv \lim_{\mathbf{q} \rightarrow 0} \lim_{\omega \rightarrow 0} \Pi_0(\mathbf{q}, \omega) = \begin{cases} -\frac{1}{4\pi} \left(\frac{2K_{F,a}m_a}{\pi} + \frac{2K_{F,b}m_b}{\pi} \right), & \text{in 3D,} \\ -\frac{1}{2\pi} (m_a + m_b), & \text{in 2D.} \end{cases} \quad (\text{S.14})$$

Eigenvectors and eigenvalues of Eq. (S.11) are numerically calculated,

$$\tilde{G}^{ex}(\mathbf{q}, \omega)^{-1} |\phi_j(\mathbf{q}, \omega)\rangle = \xi_j(\mathbf{q}, \omega) |\phi_j(\mathbf{q}, \omega)\rangle. \quad (\text{S.15})$$

The inter-band two-particle Green's function is given by the eigenvectors and eigenvalues,

$$\tilde{G}^{ex}(\mathbf{q}, \omega) = \sum_j |\phi_j(\mathbf{q}, \omega)\rangle \xi_j(\mathbf{q}, \omega)^{-1} \langle \phi_j(\mathbf{q}, \omega)|. \quad (\text{S.16})$$

Solving Eq. (S.15) numerically in 3D and 2D for general \mathbf{q} is not computationally feasible. Thus, in the next section we solve Eq. (S.15) at $\mathbf{q} = 0$, where we can employ the spherical and circular symmetry in 3D and 2D, respectively, and

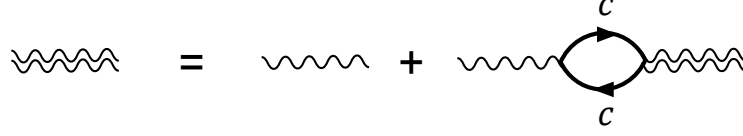


FIG. S.2. Random phase approximation (RPA) for screened Coulomb interaction. The single- and double-wavy lines are bare (long-ranged) and screened Coulomb interactions. Solid lines of bubbles correspond to free single-particle Green's functions. A bubble with label c contains a summation of bubbles consisting of free single-particle Green's functions of the a and b band ($c = a, b$).

use the irreducible representations of Eq. (S.15). From $\xi_j(\mathbf{0}, \omega)$ thus calculated, we determine exciton and antiexciton levels at the Γ point (see the next section). Then we treat small \mathbf{q} around the Γ point as a perturbation and calculate band curvatures of the exciton and antiexciton bands from the irreducible representations of Eq. (S.15) at $\mathbf{q} = 0$ (see the section after next section).

In the following, we consider the case with $K_{F,a} > K_{F,b}$ ($\mu > 0$) for clarity of presentation. A generalization to the other case is straightforward. For $|\mathbf{q}|$ smaller than $K_{F,a} - K_{F,b}$ (including $\mathbf{q} = \mathbf{0}$), the diagonal matrix $[\tilde{G}_0^{ex}(\mathbf{q}, \omega)^{-1}]_{\mathbf{k}\mathbf{k}'}$ has no finite matrix element for $K_{F,a} > |\mathbf{k} + \mathbf{q}|$ and $|\mathbf{k}| > K_{F,b}$;

$$\begin{aligned} \tilde{G}_0^{ex}(\mathbf{q}, \omega)_{\mathbf{k}\mathbf{k}'} &= \delta_{\mathbf{k}\mathbf{k}'} \left\{ \frac{\theta(|\mathbf{k} + \mathbf{q}| - K_{F,a})}{\omega - [\epsilon_a(\mathbf{k} + \mathbf{q}) - \epsilon_b(\mathbf{k})] + i0^+} - \frac{\theta(K_{F,b} - |\mathbf{k}|)}{\omega - [\epsilon_a(\mathbf{k} + \mathbf{q}) - \epsilon_b(\mathbf{k})] - i0^+} \right\}, \\ \tilde{G}_0^{ex}(\mathbf{q}, \omega)_{\mathbf{k}\mathbf{k}'}^{-1} &= \delta_{\mathbf{k}\mathbf{k}'} \begin{cases} \omega - [\epsilon_a(\mathbf{k} + \mathbf{q}) - \epsilon_b(\mathbf{k})], & |\mathbf{k} + \mathbf{q}| > K_{F,a} \\ -\{\omega - [\epsilon_a(\mathbf{k} + \mathbf{q}) - \epsilon_b(\mathbf{k})]\}, & |\mathbf{k}| < K_{F,b} \end{cases}. \end{aligned} \quad (\text{S.17})$$

Therefore, $[\tilde{G}_0^{ex}(\mathbf{q}, \omega)^{-1}]_{\mathbf{k}\mathbf{k}'}$ has finite matrix elements only within a domain of (i) $|\mathbf{k} + \mathbf{q}| > K_{F,a}$ or $K_{F,b} > |\mathbf{k}|$ and (ii) $|\mathbf{k}' + \mathbf{q}| > K_{F,a}$ or $K_{F,b} > |\mathbf{k}'|$;

$$\tilde{G}^{ex}(\mathbf{q}, \omega)^{-1} = \tilde{G}_0^{ex}(\mathbf{q}, \omega)^{-1} + \eta W \eta. \quad (\text{S.18})$$

Here η is a diagonal matrix,

$$[\eta]_{\mathbf{k}\mathbf{k}'} \equiv \delta_{\mathbf{k}\mathbf{k}'} \left[1 - \theta(K_{F,a} - |\mathbf{k} + \mathbf{q}|) \theta(|\mathbf{k}| - K_{F,b}) \right]. \quad (\text{S.19})$$

One can readily see this from a Taylor expansion of Eq. (S.11) in W in favor for \tilde{G}^{ex} ;

$$\tilde{G}^{ex} = \tilde{G}_0^{ex} - \tilde{G}_0^{ex} W \tilde{G}_0^{ex} + \tilde{G}_0^{ex} W \tilde{G}_0^{ex} W \tilde{G}_0^{ex} + \dots, \quad (\text{S.20})$$

together with $\tilde{G}_0^{ex} = \eta \tilde{G}_0^{ex} \eta$. In the next two sections, we consider to diagonalize $\tilde{G}^{ex,-1}$ within the domain.

Before closing this section, let us derive Eq. (10) in the main text using the Feynman-Hellman theorem. The ω -derivative of Eq. (S.15) at the Γ point leads to

$$\frac{d\xi_j(\mathbf{0}, \omega)}{d\omega} = \langle \phi_j(\mathbf{0}, \omega) | \left[\frac{d\tilde{G}^{ex}(\mathbf{0}, \omega)^{-1}}{d\omega} \right] | \phi_j(\mathbf{0}, \omega) \rangle, \quad (\text{S.21})$$

where $\tilde{G}^{ex}(\mathbf{0}, \omega)^{-1}$ and its ω -derivate are given by

$$\begin{aligned} [\tilde{G}^{ex}(\mathbf{0}, \omega)^{-1}]_{\mathbf{k}\mathbf{k}'} &= \delta_{\mathbf{k}\mathbf{k}'} \left\{ \theta(|\mathbf{k}| - K_{\text{out}}) \left(\omega - (\epsilon_a(\mathbf{k}) - \epsilon_b(\mathbf{k})) \right) - \theta(K_{\text{in}} - |\mathbf{k}|) \left(\omega - (\epsilon_a(\mathbf{k}) - \epsilon_b(\mathbf{k})) \right) \right\} + \frac{w(\mathbf{k} - \mathbf{k}')}{\Omega}, \\ \left[\frac{\partial}{\partial \omega} \tilde{G}^{ex}(\mathbf{0}, \omega)^{-1} \right]_{\mathbf{k}\mathbf{k}'} &= \delta_{\mathbf{k}\mathbf{k}'} \left\{ \theta(|\mathbf{k}| - K_{\text{out}}) - \theta(K_{\text{in}} - |\mathbf{k}|) \right\}. \end{aligned} \quad (\text{S.22})$$

Here $K_{\text{out}} \equiv \max(K_{F,a}, K_{F,b})$, $K_{\text{in}} \equiv \min(K_{F,a}, K_{F,b})$. From this expression, we can readily obtain Eq. (10) in the main text.

Solutions of Eqs. (S.15,S.16) at the Γ point

When $\mathbf{q} = 0$, $G^{ex}(\mathbf{0}, \omega)^{-1}$ becomes real symmetric and it has continuous spatial rotation symmetries. Eq. (S.15) can be block-diagonalized in terms of spherical harmonics in 3D and trigonometric functions in 2D. This leads to Eqs. (8,9) in the main text. In this section, we will describe this deduction and how the radial functions in Eqs. (8,9) in the main text should be calculated. With $\overline{G^{ex}}(\mathbf{q}, \omega; \mathbf{k}, \mathbf{k}') \equiv \Omega \tilde{G}^{ex}(\mathbf{q}, \omega)_{\mathbf{k}\mathbf{k}'}$, the BS equation at $\mathbf{q} = 0$ is given by

$$\int \frac{d^d \mathbf{k}''}{(2\pi)^d} \left(D(\omega; \mathbf{k})(2\pi)^d \delta(\mathbf{k} - \mathbf{k}'') + w(\mathbf{k} - \mathbf{k}'') \right) \overline{G^{ex}}(\mathbf{0}, \omega; \mathbf{k}'', \mathbf{k}') = (2\pi)^d \delta(\mathbf{k} - \mathbf{k}'), \quad (\text{S.23})$$

and

$$D(\omega; \mathbf{k}) = \theta(|\mathbf{k}| - K_{\text{out}}) \left(\omega - (\epsilon_a(\mathbf{k}) - \epsilon_b(\mathbf{k})) \right) - \theta(K_{\text{in}} - |\mathbf{k}|) \left(\omega - (\epsilon_a(\mathbf{k}) - \epsilon_b(\mathbf{k})) \right). \quad (\text{S.24})$$

Note that any momentum index \mathbf{k} in the equations is confined to be in a range $|\mathbf{k}| > K_{\text{out}}$ or $|\mathbf{k}| < K_{\text{in}}$. $\tilde{G}^{ex}(\mathbf{q}, \omega)_{\mathbf{k}\mathbf{k}'} = 0$ if \mathbf{k} or \mathbf{k}' is outside the range.

• In the 3D case, the delta function in the right hand side of Eq. (S.23) as well as the screened Coulomb interaction can be decomposed in terms of the spherical harmonics,

$$\delta(\mathbf{k} - \mathbf{k}') = \frac{1}{k^2} \delta(k - k') \delta(\cos \theta - \cos \theta') \delta(\varphi - \varphi') = \frac{1}{k^2} \delta(k - k') \sum_{lm} Y_{lm}(\theta, \varphi) Y_{lm}^*(\theta', \varphi'), \quad (\text{S.25})$$

$$w(\mathbf{k} - \mathbf{k}') = \frac{4\pi}{k^2 + k'^2 - 2kk' \cos \gamma + k_{TF}^2} = \sum_l a_l(k, k') P_l(\cos \gamma) = \sum_{lm} a_l(k, k') \frac{4\pi}{2l+1} Y_{lm}(\theta, \varphi) Y_{lm}^*(\theta', \varphi'). \quad (\text{S.26})$$

Here $\mathbf{k} \equiv (k \sin \theta \cos \varphi, k \sin \theta \sin \varphi, k \cos \theta)$. γ is an angle between \mathbf{k} and \mathbf{k}' . $P_l(\cos \gamma)$ is the Legendre polynomial ($l = 0, 1, \dots$). $Y_{lm}(\theta, \varphi)$ is the spherical harmonics ($m = -l, -l+1, \dots, l$). The spherical harmonics are defined with normalization and completeness relations,

$$\int_{-1}^1 d(\cos \theta) \int_0^{2\pi} d\varphi Y_{lm}^*(\theta, \varphi) Y_{l'm'}(\theta, \varphi) = \delta_{ll'} \delta_{mm'}, \quad \sum_{lm} Y_{lm}(\theta, \varphi) Y_{lm}^*(\theta', \varphi') = \delta(\cos \theta - \cos \theta') \delta(\varphi - \varphi'). \quad (\text{S.27})$$

$a_l(k, k')$ is the coefficient of the Legendre expansion. The lowest and second lowest order coefficients are calculated as

$$a_0(k, k') = \frac{\pi}{kk'} \left\{ \ln \left((k+k')^2 + k_{TF}^2 \right) - \ln \left((k-k')^2 + k_{TF}^2 \right) \right\}, \quad (\text{S.28})$$

$$a_1(k, k') = \frac{3\pi}{kk'} \left\{ \frac{k^2 + k'^2 + k_{TF}^2}{2kk'} \left[\ln \left((k+k')^2 + k_{TF}^2 \right) - \ln \left((k-k')^2 + k_{TF}^2 \right) \right] - 2 \right\}. \quad (\text{S.29})$$

In terms of the harmonics, the solution of Eq. (S.23) is given by

$$\overline{G^{ex}}(\mathbf{0}, \omega; \mathbf{k}'', \mathbf{k}') = \sum_{nlm} \frac{Y_{lm}(\theta'', \varphi'') f_{nl}(\omega; k'') f_{nl}(\omega; k') Y_{lm}^*(\theta', \varphi')}{\xi_{nl}(\omega)}. \quad (\text{S.30})$$

Here $f_{nl}(\omega; k)$ and $\xi_{nl}(\omega)$ are eigenvector and eigenvalue of a one-dimensional integral equation,

$$\int_0^\infty \frac{k'^2 dk'}{(2\pi)^3} h_l(\omega; k, k') f_{nl}(\omega; k') = \xi_{nl}(\omega) f_{nl}(\omega; k), \quad (\text{S.31})$$

with

$$h_l(\omega; k, k') \equiv \frac{D(\omega; k)}{k^2} (2\pi)^3 \delta(k - k') + \frac{4\pi}{2l+1} a_l(k, k'), \quad (\text{S.32})$$

and normalization and completeness relations,

$$\sum_n f_{nl}(\omega; k) f_{nl}(\omega; k') = \frac{(2\pi)^3}{k^2} \delta(k - k'), \quad \int_0^\infty \frac{k^2 dk}{(2\pi)^3} f_{nl}(\omega; k) f_{n'l}(\omega; k) = \delta_{nn'}. \quad (\text{S.33})$$

To solve the one-dimensional integral equation numerically, k is discretized by $2\pi/L$ with large L ;

$$\int_0^\infty dk = \frac{2\pi}{L} \sum_k, \quad \delta(k - k') = \frac{L}{2\pi} \delta_{kk'}. \quad (\text{S.34})$$

With the discretization, the integral equation takes a form of

$$\sum_{k'} H_{l,kk'}^\omega V_{nl,k'}^\omega = \xi_{nl}(\omega) V_{nl,k}^\omega, \quad (\text{S.35})$$

where

$$H_{l,kk'}^\omega \equiv D(\omega; k) \delta_{kk'} + \frac{1}{L} \frac{kk'}{\pi} \frac{a_l(k, k')}{2l+1}, \quad V_{nl,k}^\omega \equiv \frac{k}{2\pi\sqrt{L}} f_{nl}(\omega; k). \quad (\text{S.36})$$

Here $V_{nl,k}^\omega$ satisfies $\sum_k V_{nl,k}^\omega V_{n'l,k}^\omega = \delta_{nn'}$ and $\sum_n V_{nl,k}^\omega V_{nl,k'}^\omega = \delta_{kk'}$.

• In the 2D case, the delta function and the screened Coulomb interaction are expanded in terms of the trigonometric functions,

$$\delta(\mathbf{k} - \mathbf{k}') = \frac{\delta(k - k')}{k} \delta(\varphi - \varphi') = \frac{\delta(k - k')}{k} \frac{1}{2\pi} \sum_m e^{im(\varphi - \varphi')}, \quad (\text{S.37})$$

$$w(\mathbf{k} - \mathbf{k}') = \frac{2\pi}{\sqrt{k^2 + k'^2 - 2kk' \cos(\varphi - \varphi')} + k_{TF}} = \sum_m F_m(k, k') e^{im(\varphi - \varphi')}, \quad (\text{S.38})$$

where $\mathbf{k} \equiv (k \cos \varphi, k \sin \varphi)$, and

$$F_m(k, k') = \int_0^\pi d\phi \frac{2 \cos(m\phi)}{\sqrt{k^2 + k'^2 - 2kk' \cos \phi} + k_{TF}}. \quad (\text{S.39})$$

In terms of the expansion, the solution of Eq. (S.23) is given by

$$\overline{G^{ex}}(\mathbf{0}, \omega; \mathbf{k}'', \mathbf{k}') = \sum_{nm} \frac{f_{nm}(\omega; k'') f_{nm}(\omega; k') e^{im(\varphi'' - \varphi')}}{\xi_{nm}(\omega)}. \quad (\text{S.40})$$

Here $f_{nm}(\omega; k)$ and $\xi_{nm}(\omega)$ are the eigenvector and eigenvalue of a one-dimensional integral equation,

$$\int_0^{+\infty} \frac{k' dk'}{2\pi} h_m(\omega; k, k') f_{nm}(\omega; k') = \xi_{nm}(\omega) f_{nm}(\omega; k), \quad (\text{S.41})$$

with

$$h_m(\omega; k, k') = \frac{D(\omega; k)}{k} (2\pi) \delta(k - k') + F_m(k, k'), \quad (\text{S.42})$$

and normalization and completeness relation

$$\sum_n f_{nm}(\omega; k) f_{nm}(\omega; k') = \frac{2\pi}{k} \delta(k - k'), \quad \int_0^{+\infty} \frac{k dk}{2\pi} f_{nm}(\omega; k) f_{n'm'}(\omega, k) = \delta_{nn'}. \quad (\text{S.43})$$

With the same discretization as Eq. (S.34), the integral equation reduces to

$$\sum_{k'} H_{m,kk'}^\omega V_{nm,k'}^\omega = \xi_{nm}(\omega) V_{nm,k}^\omega, \quad (\text{S.44})$$

where

$$H_{m,kk'}^\omega \equiv D(\omega; k) \delta_{kk'} + \frac{\sqrt{kk'}}{L} F_m(k, k'), \quad V_{nm,k}^\omega \equiv \sqrt{\frac{k}{L}} f_{nm}(\omega; k). \quad (\text{S.45})$$

Here $V_{nm,k}^\omega$ satisfies $\sum_k V_{nm,k}^\omega V_{n'm,k}^\omega = \delta_{nn'}$ and $\sum_n V_{nm,k}^\omega V_{nm,k'}^\omega = \delta_{kk'}$. $F_m(k, k')$ in Eq. (S.39) is evaluated numerically.

In the numerical diagonalization of Eqs. (S.35, S.44), we set a large value of L ($\sim 300 \times 2\pi$) and a large cutoff of k ($> 15 \times \max(K_{F,a}, K_{F,b})$) so that the numerical solutions of the eigenvalues are convergent.

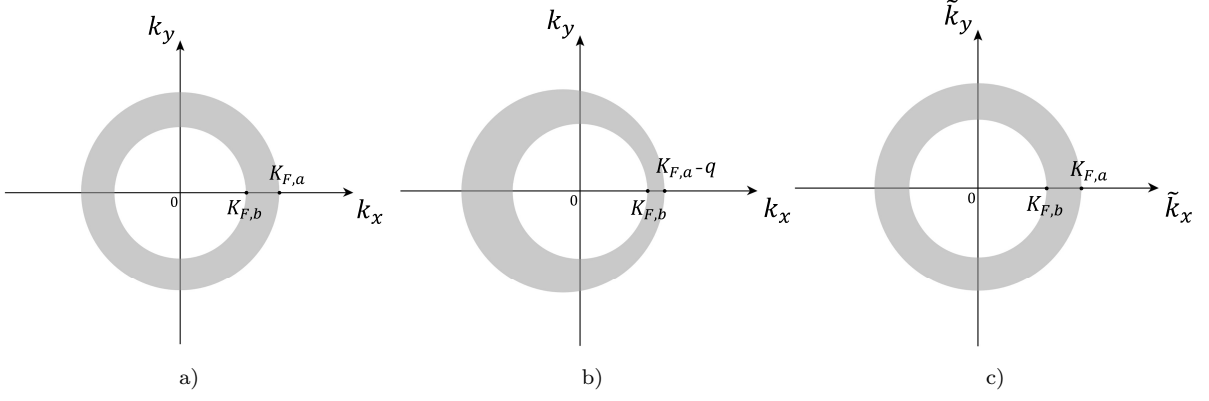


FIG. S.3. The shaded regions are excluded for the domains of \mathbf{k} and \mathbf{k}' for $[\tilde{G}^{ex}(\mathbf{0}, \omega)^{-1}]_{\mathbf{k}\mathbf{k}'}$ (a), \mathbf{k} and \mathbf{k}' for $[\tilde{G}^{ex}(\mathbf{q}, \omega)^{-1}]_{\mathbf{k}\mathbf{k}'}$ (b), and $\tilde{\mathbf{k}}$ and $\tilde{\mathbf{k}}'$ for $[\tilde{G}^{ex}(\mathbf{q}, \omega)^{-1}]_{\tilde{\mathbf{k}}\tilde{\mathbf{k}}'}$ (c). We take $\mathbf{q} = q\mathbf{e}_x$ in the figure. The figures are plotted in the xy plane. For 3D, the y and z directions are symmetric.

Calculation of the band curvatures of exciton and antiexciton bands around the Γ point

The previous section describes how to evaluate exciton and antiexciton band energies at the Γ point. This section describes how to evaluate energy-band curvatures of the exciton and antiexciton bands around the Γ point. Let us begin with Eq. (S.15),

$$\sum_{\mathbf{k}'} [\tilde{G}^{ex}(\mathbf{q}, \omega)^{-1}]_{\mathbf{k}\mathbf{k}'} \langle \mathbf{k}' | \phi_j(\mathbf{q}, \omega) \rangle = \xi_j(\mathbf{q}, \omega) \langle \mathbf{k} | \phi_j(\mathbf{q}, \omega) \rangle. \quad (\text{S.46})$$

The eigenvalue problem at $\mathbf{q} = 0$ is supposed to be solved for the 3D and 2D case respectively (see the previous section);

$$\sum_{\mathbf{k}'} [\tilde{G}^{ex}(\mathbf{0}, \omega)^{-1}]_{\mathbf{k}\mathbf{k}'} \langle \mathbf{k}' | \phi_j(\mathbf{0}, \omega) \rangle = \xi_j(\mathbf{0}, \omega) \langle \mathbf{k} | \phi_j(\mathbf{0}, \omega) \rangle, \quad (\text{S.47})$$

with a normalization,

$$\langle \mathbf{k} | \phi_j(\mathbf{q} = 0, \omega) \rangle = \begin{cases} \frac{1}{\sqrt{\Omega}} f_{nl}(\omega; k) Y_{lm}(\theta, \varphi), & j = (nlm), \text{ in 3D,} \\ \frac{1}{\sqrt{\Omega}} f_{nm}(\omega; k) e^{im\varphi}, & j = (nm), \text{ in 2D.} \end{cases} \quad (\text{S.48})$$

The normalization gives a proper completeness relation,

$$\sum_j \langle \mathbf{k} | \phi_j(\mathbf{0}, \omega) \rangle \langle \phi_j(\mathbf{0}, \omega) | \mathbf{k}' \rangle = \delta_{\mathbf{k}\mathbf{k}'}, \quad \sum_{\mathbf{k}} \langle \phi_j(\mathbf{0}, \omega) | \mathbf{k} \rangle \langle \mathbf{k} | \phi_{j'}(\mathbf{0}, \omega) \rangle = \delta_{jj'}. \quad (\text{S.49})$$

To obtain the band curvature around the Γ point, we consider $|\mathbf{q}|$ as a small quantity, expand $\tilde{G}^{ex}(\mathbf{q}, \omega)^{-1}$ in \mathbf{q} up to the second order, and evaluate the second-order energy correction of $\xi_j(\mathbf{q}, \omega)$; $\xi_j(\mathbf{q}, \omega) = \xi_j(\mathbf{0}, \omega) + b(\omega)q^2$. By the rotational symmetry, a q -linear energy correction is zero, while the q -quadratic energy correction depends only on the norm of \mathbf{q} , $q \equiv |\mathbf{q}|$.

Note that the domain of \mathbf{k} and \mathbf{k}' for $[\tilde{G}^{ex}(\mathbf{q}, \omega)^{-1}]_{\mathbf{k}\mathbf{k}'}$ (Fig. S.3(a)) and that for $[\tilde{G}^{ex}(\mathbf{0}, \omega)^{-1}]_{\mathbf{k}\mathbf{k}'}$ (Fig. S.3(b)) are different from each other. To adjust these two domains, we define the following two new variables as replacements of \mathbf{k} and \mathbf{k}' , respectively,

$$\tilde{\mathbf{k}} \equiv \begin{cases} \mathbf{k} + \mathbf{q}, & |\mathbf{k} + \mathbf{q}| > K_{F,a} \\ \mathbf{k}, & |\mathbf{k}| < K_{F,b} \end{cases}, \quad \tilde{\mathbf{k}}' \equiv \begin{cases} \mathbf{k}' + \mathbf{q}, & |\mathbf{k}' + \mathbf{q}| > K_{F,a} \\ \mathbf{k}', & |\mathbf{k}'| < K_{F,b} \end{cases}. \quad (\text{S.50})$$

In terms of the new variables, $[\tilde{G}^{ex}(\mathbf{q}, \omega)^{-1}]_{\tilde{\mathbf{k}}\tilde{\mathbf{k}}'}$ shares the identical domain (Fig. S.3(c)) with $[\tilde{G}^{ex}(\mathbf{0}, \omega)^{-1}]_{\tilde{\mathbf{k}}\tilde{\mathbf{k}}'}$; (i) $|\tilde{\mathbf{k}}| > K_{F,a}$ or $K_{F,b} > |\tilde{\mathbf{k}}|$ and (ii) $|\tilde{\mathbf{k}}'| > K_{F,a}$ or $K_{F,b} > |\tilde{\mathbf{k}}'|$. Let us compare their matrix elements in the domain. In

terms of the new variables, $\tilde{G}^{ex,-1} = \tilde{G}_0^{ex,-1} + W$ is given by

$$[\tilde{G}_0^{ex,-1}(\mathbf{q}, \omega)]_{\tilde{\mathbf{k}}\tilde{\mathbf{k}}'} = \delta_{\tilde{\mathbf{k}}\tilde{\mathbf{k}}'} \begin{cases} \omega - [\epsilon_a(\tilde{\mathbf{k}}) - \epsilon_b(\tilde{\mathbf{k}} - \mathbf{q})], & |\tilde{\mathbf{k}}| > K_{F,a} \\ -\{\omega - [\epsilon_a(\tilde{\mathbf{k}} + \mathbf{q}) - \epsilon_b(\tilde{\mathbf{k}})]\}, & |\tilde{\mathbf{k}}| < K_{F,b} \end{cases}, \quad (\text{S.51})$$

$$[W]_{\tilde{\mathbf{k}}\tilde{\mathbf{k}}'} = \begin{cases} \frac{w(\tilde{\mathbf{k}} - \tilde{\mathbf{k}}')}{\Omega} & |\tilde{\mathbf{k}}| > K_{F,a}, \quad |\tilde{\mathbf{k}}'| > K_{F,a} \\ \frac{w(\tilde{\mathbf{k}} - \tilde{\mathbf{k}}')}{\Omega} & |\tilde{\mathbf{k}}| < K_{F,b}, \quad |\tilde{\mathbf{k}}'| < K_{F,b} \\ \frac{w(\tilde{\mathbf{k}} - \mathbf{q} - \tilde{\mathbf{k}}')}{\Omega} & |\tilde{\mathbf{k}}| > K_{F,a}, \quad |\tilde{\mathbf{k}}'| < K_{F,b} \\ \frac{w(\tilde{\mathbf{k}} - \tilde{\mathbf{k}}' + \mathbf{q})}{\Omega} & |\tilde{\mathbf{k}}| < K_{F,b}, \quad |\tilde{\mathbf{k}}'| > K_{F,a} \end{cases}. \quad (\text{S.52})$$

In the following, we take $\mathbf{q} = q\mathbf{e}_i$ (\mathbf{e}_i is a unit vector along i , $i = x, y, z$) and take q -derivatives of the $\tilde{G}^{ex}(\mathbf{q}, \omega)_{\tilde{\mathbf{k}}\tilde{\mathbf{k}}'}^{-1}$ matrix around the $\mathbf{q} = 0$ point.

For simplicity of the presentation, let us call the new variables $\tilde{\mathbf{k}}$ and $\tilde{\mathbf{k}}'$ as \mathbf{k} and \mathbf{k}' . The first q -derivative of $\tilde{G}^{ex}(\mathbf{q}, \omega)_{\mathbf{k}\mathbf{k}'}^{-1}$ is given by

$$[\mathbf{F}_i]_{\mathbf{k}\mathbf{k}'} \equiv \left[\frac{\partial \tilde{G}^{ex}(q\mathbf{e}_i, \omega)^{-1}}{\partial q} \Big|_{q=0} \right]_{\mathbf{k}\mathbf{k}'} = \begin{cases} \frac{k_i}{m_b} & |\mathbf{k}| > K_{F,a}, \quad \mathbf{k} = \mathbf{k}' \\ \frac{k_i}{m_a} & |\mathbf{k}| < K_{F,b}, \quad \mathbf{k} = \mathbf{k}' \\ 0 & |\mathbf{k}| < K_{F,b}, \quad |\mathbf{k}'| < K_{F,b}, \quad \mathbf{k} \neq \mathbf{k}' \\ 0 & |\mathbf{k}| > K_{F,a}, \quad |\mathbf{k}'| > K_{F,a}, \quad \mathbf{k} \neq \mathbf{k}' \\ \frac{1}{\Omega} \frac{\partial w(\mathbf{k} - \mathbf{k}' + q\mathbf{e}_i)}{\partial q} \Big|_{q=0} & |\mathbf{k}| < K_{F,b}, \quad |\mathbf{k}'| > K_{F,a} \\ \frac{1}{\Omega} \frac{\partial w(\mathbf{k} - q\mathbf{e}_i - \mathbf{k}')}{\partial q} \Big|_{q=0} & |\mathbf{k}| > K_{F,a}, \quad |\mathbf{k}'| < K_{F,b} \end{cases}, \quad (\text{S.53})$$

with

$$\frac{\partial w(\mathbf{k} - \mathbf{k}' + q\mathbf{e}_i)}{\partial q} \Big|_{q=0} = \begin{cases} -\frac{4\pi \times 2(k_i - k'_i)}{(|\mathbf{k} - \mathbf{k}'|^2 + k_{TF}^2)^2} & \text{in 3D,} \\ -\frac{2\pi}{(|\mathbf{k} - \mathbf{k}'| + k_{TF})^2} \frac{k_i - k'_i}{|\mathbf{k} - \mathbf{k}'|} & \text{in 2D.} \end{cases} \quad (\text{S.54})$$

The second q -derivative of $\tilde{G}^{ex}(\mathbf{q}, \omega)_{\mathbf{k}\mathbf{k}'}^{-1}$ is given by

$$2[\mathbf{S}_i]_{\mathbf{k}\mathbf{k}'} \equiv \left[\frac{\partial^2 \tilde{G}^{ex}(q\mathbf{e}_i, \omega)^{-1}}{\partial q^2} \Big|_{q=0} \right]_{\mathbf{k}\mathbf{k}'} = \begin{cases} -\frac{1}{m_b} & |\mathbf{k}| > K_{F,a}, \quad \mathbf{k} = \mathbf{k}' \\ \frac{1}{m_a} & |\mathbf{k}| < K_{F,b}, \quad \mathbf{k} = \mathbf{k}' \\ 0 & |\mathbf{k}| < K_{F,b}, \quad |\mathbf{k}'| < K_{F,b}, \quad \mathbf{k} \neq \mathbf{k}' \\ 0 & |\mathbf{k}| > K_{F,a}, \quad |\mathbf{k}'| > K_{F,a}, \quad \mathbf{k} \neq \mathbf{k}' \\ \frac{1}{\Omega} \frac{\partial^2 w(\mathbf{k} - \mathbf{k}' + q\mathbf{e}_i)}{\partial q^2} \Big|_{q=0} & |\mathbf{k}| < K_{F,b}, \quad |\mathbf{k}'| > K_{F,a} \\ \frac{1}{\Omega} \frac{\partial^2 w(\mathbf{k} - q\mathbf{e}_i - \mathbf{k}')}{\partial q^2} \Big|_{q=0} & |\mathbf{k}| > K_{F,a}, \quad |\mathbf{k}'| < K_{F,b} \end{cases}, \quad (\text{S.55})$$

with

$$\frac{\partial^2 w(\mathbf{k} - \mathbf{k}' + q\mathbf{e}_i)}{\partial q^2} \Big|_{q=0} = \begin{cases} -\frac{4\pi \times 2}{(|\mathbf{k} - \mathbf{k}'|^2 + k_{TF}^2)^2} + \frac{4\pi \times 2 \times 4(k_i - k'_i)^2}{(|\mathbf{k} - \mathbf{k}'|^2 + k_{TF}^2)^3} & \text{in 3D,} \\ -\frac{2\pi}{(|\mathbf{k} - \mathbf{k}'| + k_{TF})^2} \frac{1}{|\mathbf{k} - \mathbf{k}'|} + \frac{2\pi \times 2}{(|\mathbf{k} - \mathbf{k}'| + k_{TF})^3} \frac{(k_i - k'_i)^2}{|\mathbf{k} - \mathbf{k}'|^2} + \frac{2\pi}{(|\mathbf{k} - \mathbf{k}'| + k_{TF})^2} \frac{(k_i - k'_i)^2}{|\mathbf{k} - \mathbf{k}'|^3} & \text{in 2D.} \end{cases} \quad (\text{S.56})$$

Now that $\tilde{G}^{ex}(q\mathbf{e}_i, \omega)^{-1}$ is expanded in q ,

$$[\tilde{G}^{ex}(q\mathbf{e}_i, \omega)^{-1}] = [\tilde{G}^{ex}(\mathbf{0}, \omega)^{-1}] + [\mathbf{F}_i]q + [\mathbf{S}_i]q^2 + \mathcal{O}(q^3), \quad (\text{S.57})$$

the second-order perturbation theory gives the second-order energy correction,

$$\xi_j(q\mathbf{e}_i, \omega) = \xi_j(\mathbf{0}, \omega) + b_j(\omega)q^2 + \mathcal{O}(q^3). \quad (\text{S.58})$$

Here $b_j(\omega)$ is given by the eigenvectors and eigenvalues at $\mathbf{q} = 0$ (See Eqs. (S.47, S.48)),

$$b_j(\omega) = \sum_{j' \neq j} \frac{\langle \phi_j(\mathbf{0}, \omega) | \mathbf{F}_i | \phi_{j'}(\mathbf{0}, \omega) \rangle \langle \phi_{j'}(\mathbf{0}, \omega) | \mathbf{F}_i | \phi_j(\mathbf{0}, \omega) \rangle}{\xi_j(\mathbf{0}, \omega) - \xi_{j'}(\mathbf{0}, \omega)} + \langle \phi_j(\mathbf{0}, \omega) | \mathbf{S}_i | \phi_j(\mathbf{0}, \omega) \rangle \equiv F_2 + S_1. \quad (\text{S.59})$$

The previous section describes how to calculate the eigenvectors and eigenvalues of the lowest-energy s -wave exciton and antiexciton at $\mathbf{q} = 0$ in the 3D case ($j \equiv (nlm) = (100)$) and 2D case ($j = (nm) = (10)$). In the following, we will describe how to calculate $b_{(100)}(\omega = \pm\omega_{\pm})$ in the 3D case and $b_{(10)}(\omega = \pm\omega_{\pm})$ in the 2D case.

- In 3D, $j \equiv (nlm)$. Take $(nlm) = (100)$ and $\mathbf{e}_i = \mathbf{e}_z$. Since $\xi_j(\mathbf{q} = \mathbf{0}, \omega = \pm\omega_{\pm}) = 0$, F_2 is given by

$$F_2 = - \sum_{nlm \neq (100)} \sum_{\mathbf{k}_1, \mathbf{k}_2, \mathbf{k}_3, \mathbf{k}_4} \frac{\langle \phi_{100}(\mathbf{0}, \omega) | \mathbf{k}_1 \rangle [\mathbf{F}_z]_{\mathbf{k}_1 \mathbf{k}_2} \langle \mathbf{k}_2 | \phi_{nlm}(\mathbf{0}, \omega) \rangle \langle \phi_{nlm}(\mathbf{0}, \omega) | \mathbf{k}_3 \rangle [\mathbf{F}_z]_{\mathbf{k}_3 \mathbf{k}_4} \langle \mathbf{k}_4 | \phi_{100}(\mathbf{0}, \omega) \rangle}{\xi_{nl}(\mathbf{0}, \omega)}. \quad (\text{S.60})$$

In terms of Eq. (S.48) and $Y_{00}(\theta, \varphi) = \frac{1}{2\sqrt{\pi}}$, we evaluate matrix elements of \mathbf{F}_z by three-dimensional momentum integrals;

$$\begin{aligned} \sum_{\mathbf{k}_1, \mathbf{k}_2} \langle \phi_{100}(\mathbf{0}, \omega) | \mathbf{k}_1 \rangle [\mathbf{F}_z]_{\mathbf{k}_1 \mathbf{k}_2} \langle \mathbf{k}_2 | \phi_{nlm}(\mathbf{0}, \omega) \rangle &= \left(\prod_{i=1}^2 \int_0^{+\infty} \frac{dk_i}{(2\pi)^3} k_i^2 \int_{-1}^1 d \cos \theta_i \int_0^{2\pi} d\varphi_i \right) \\ & f_{10}(\omega; k_1) \frac{1}{2\sqrt{\pi}} \Omega[\mathbf{F}_z]_{\mathbf{k}_1 \mathbf{k}_2} f_{nl}(\omega; k_2) Y_{lm}(\theta_2, \varphi_2), \end{aligned} \quad (\text{S.61})$$

with

$$\begin{aligned} \Omega[\mathbf{F}_z]_{\mathbf{k}_1 \mathbf{k}_2} &= \left(\theta(k_1 - K_{F,a}) \frac{k_1 \cos \theta_1}{m_b} + \theta(K_{F,b} - k_1) \frac{k_1 \cos \theta_1}{m_a} \right) \frac{(2\pi)^3}{k_1^2} \delta(k_1 - k_2) \sum_{lm} Y_{lm}(\theta_1, \varphi_1) Y_{lm}^*(\theta_2, \varphi_2) \\ &+ 2 \sum_{lm} b_l(k_1, k_2) \frac{4\pi}{2l+1} Y_{lm}(\theta_1, \varphi_1) Y_{lm}^*(\theta_2, \varphi_2) \left(\theta(k_1 - K_{F,a}) \theta(K_{F,b} - k_2) (k_1 \cos \theta_1 - k_2 \cos \theta_2) \right. \\ &\quad \left. + \theta(k_2 - K_{F,a}) \theta(K_{F,b} - k_1) (k_2 \cos \theta_2 - k_1 \cos \theta_1) \right). \end{aligned} \quad (\text{S.62})$$

Here $\mathbf{k}_j \equiv k_j(\sin \theta_j \cos \varphi_j, \sin \theta_j \sin \varphi_j, \cos \theta_j)$ ($j = 1, 2, 3, 4$) and we used the spherical expansion of Eq. (S.54);

$$\frac{4\pi}{(|\mathbf{k}_1 - \mathbf{k}_2|^2 + k_{TF}^2)^2} = \sum_l b_l(k_1, k_2) P_l(\cos \gamma) = \sum_{lm} b_l(k_1, k_2) \frac{4\pi}{2l+1} Y_{lm}(\theta_1, \varphi_1) Y_{lm}^*(\theta_2, \varphi_2). \quad (\text{S.63})$$

The lowest and second lowest expansion coefficients are calculated as

$$b_0(k_1, k_2) = \frac{\pi}{k_1 k_2} \left(\frac{1}{(k_1 - k_2)^2 + k_{TF}^2} - \frac{1}{(k_1 + k_2)^2 + k_{TF}^2} \right), \quad (\text{S.64})$$

$$b_1(k_1, k_2) = \frac{3\pi}{2(k_1 k_2)^2} \left\{ \ln \left[\frac{(k_1 - k_2)^2 + k_{TF}^2}{(k_1 + k_2)^2 + k_{TF}^2} \right] + (k_1^2 + k_2^2 + k_{TF}^2) \left[\frac{1}{(k_1 - k_2)^2 + k_{TF}^2} - \frac{1}{(k_1 + k_2)^2 + k_{TF}^2} \right] \right\}. \quad (\text{S.65})$$

Under the momentum integrals, only $(lm) = (10)$ term remains finite in Eq. (S.61). With $\cos \theta = 2\sqrt{\frac{\pi}{3}} Y_{10}^*(\theta, \varphi)$, the non-zero term is evaluated as

$$\langle \phi_{100}(\mathbf{0}, \omega) | \mathbf{F}_z | \phi_{nlm}(\mathbf{0}, \omega) \rangle = \delta_{l1} \delta_{m0} \left(\prod_{i=1}^2 \int_0^{+\infty} \frac{dk_i}{(2\pi)^3} k_i^2 \right) \frac{1}{2\sqrt{\pi}} 2\sqrt{\frac{\pi}{3}} f_{10}(\omega; k_1) \rho(k_1, k_2) f_{n1}(\omega; k_2), \quad (\text{S.66})$$

with

$$\begin{aligned} \rho(k_1, k_2) &= \left(\theta(k_1 - K_{F,a}) \frac{k_1}{m_b} + \theta(K_{F,b} - k_1) \frac{k_1}{m_a} \right) (2\pi)^3 \frac{\delta(k_1 - k_2)}{k_1^2} \\ &+ 2 \left(\theta(k_1 - K_{F,a}) \theta(K_{F,b} - k_2) \left(\frac{4\pi}{3} b_1(k_1, k_2) k_1 - 4\pi b_0(k_1, k_2) k_2 \right) \right. \\ &\quad \left. + \theta(k_2 - K_{F,a}) \theta(K_{F,b} - k_1) \left(4\pi b_0(k_1, k_2) k_2 - \frac{4\pi}{3} b_1(k_1, k_2) k_1 \right) \right). \end{aligned} \quad (\text{S.67})$$

Then we finally have

$$F_2 = - \left(\prod_{i=1}^4 \int_0^{+\infty} \frac{dk_i}{(2\pi)^3} k_i^2 \right) \left(\frac{1}{2\sqrt{\pi}} 2\sqrt{\frac{\pi}{3}} \right)^2 \sum_n \frac{1}{\xi_{n1}(\mathbf{0}, \omega)} f_{10}(\omega; k_1) \rho(k_1, k_2) f_{n1}(\omega; k_2) f_{n1}(\omega; k_3) \rho(k_3, k_4) f_{10}(\omega; k_4). \quad (\text{S.68})$$

To numerically evaluate Eq. (S.68), we use the same discretization of k as in Eq. (S.34),

$$\begin{aligned} F_2 &= -\frac{1}{3} \sum_{k_1, k_2, k_3, k_4} \sum_n V_{10, k_1}^\omega P_{k_1 k_2} V_{n1, k_2}^\omega \frac{1}{\xi_{n1}(\mathbf{0}, \omega)} V_{n1, k_3}^\omega P_{k_3 k_4} V_{10, k_4}^\omega \\ &= -\frac{1}{3} \sum_{k_1, k_2, k_3, k_4} V_{10, k_1}^\omega P_{k_1 k_2} H_{1, k_2 k_3}^{\omega, -1} P_{k_3 k_4} V_{10, k_4}^\omega. \end{aligned} \quad (\text{S.69})$$

$V_{nl, k}^\omega$ and $H_{1, k k'}^\omega$ are defined in Eq. (S.36) and

$$\begin{aligned} P_{k_1 k_2} &= \frac{k_1 k_2}{L(2\pi)^2} \rho(k_1, k_2) = \left(\theta(k_1 - K_{F,a}) \frac{k_1}{m_b} + \theta(K_{F,b} - k_1) \frac{k_1}{m_a} \right) \delta_{k_1 k_2} \\ &\quad + \frac{2k_1 k_2}{L(2\pi)^2} \left(\theta(k_1 - K_{F,a}) \theta(K_{F,b} - k_2) \left(\frac{4\pi}{3} b_1(k_1, k_2) k_1 - 4\pi b_0(k_1, k_2) k_2 \right) \right. \\ &\quad \left. + \theta(k_2 - K_{F,a}) \theta(K_{F,b} - k_1) \left(4\pi b_0(k_1, k_2) k_2 - \frac{4\pi}{3} b_1(k_1, k_2) k_1 \right) \right). \end{aligned} \quad (\text{S.70})$$

S_1 in Eq. (S.59) is given by

$$\begin{aligned} S_1 &= \sum_{\mathbf{k}_1, \mathbf{k}_2} \langle \phi_{100}(\mathbf{0}, \omega) | \mathbf{k}_1 \rangle [\mathbf{S}_z]_{\mathbf{k}_1, \mathbf{k}_2} \langle \mathbf{k}_2 | \phi_{100}(\mathbf{0}, \omega) \rangle = \frac{1}{3} \sum_{\mathbf{k}_1, \mathbf{k}_2} \langle \phi_{100}(\mathbf{0}, \omega) | \mathbf{k}_1 \rangle [\mathbf{S}_z + \mathbf{S}_x + \mathbf{S}_y]_{\mathbf{k}_1, \mathbf{k}_2} \langle \mathbf{k}_2 | \phi_{100}(\mathbf{0}, \omega) \rangle \\ &= \left(\prod_{i=1}^2 \int_0^{+\infty} \frac{dk_i}{(2\pi)^3} \right) k_i^2 \int_{-1}^1 d \cos \theta_i \int_0^{2\pi} d\varphi_i \frac{1}{2\sqrt{\pi}} f_{10}(\omega; k_1) \Omega \mathbf{S}(\mathbf{k}_1, \mathbf{k}_2) f_{10}(\omega; k_2) \frac{1}{2\sqrt{\pi}}, \end{aligned} \quad (\text{S.71})$$

with

$$\begin{aligned} \Omega \mathbf{S}(\mathbf{k}_1, \mathbf{k}_2) &= \left(\theta(k_1 - K_{F,a}) \frac{-1}{2m_b} + \theta(K_{F,b} - k_1) \frac{1}{2m_a} \right) \frac{(2\pi)^3}{k_1^2} \delta(k_1 - k_2) \sum_{lm} Y_{lm}(\theta_1, \varphi_1) Y_{lm}^*(\theta_2, \varphi_2) \\ &\quad + \sum_{lm} \beta_l(k_1, k_2) \frac{4\pi}{2l+1} Y_{lm}(\theta_1, \varphi_1) Y_{lm}^*(\theta_2, \varphi_2) \left(\theta(k_1 - K_{F,a}) \theta(K_{F,b} - k_2) + \theta(k_2 - K_{F,a}) \theta(K_{F,b} - k_1) \right). \end{aligned} \quad (\text{S.72})$$

Here we used the spherical expansion of Eq. (S.56);

$$-\frac{4\pi}{(|\mathbf{k}_1 - \mathbf{k}_2|^2 + k_{TF}^2)^2} + \frac{4\pi \times 4|\mathbf{k}_1 - \mathbf{k}_2|^2/3}{(|\mathbf{k}_1 - \mathbf{k}_2|^2 + k_{TF}^2)^3} = \sum_{lm} \beta_l(k_1, k_2) \frac{4\pi}{2l+1} Y_{lm}(\theta_1, \varphi_1) Y_{lm}^*(\theta_2, \varphi_2). \quad (\text{S.73})$$

The lowest order expansion coefficient is calculated as

$$\beta_0(k_1, k_2) = \frac{\pi}{3k_1 k_2} \left(\frac{1}{(k_1 - k_2)^2 + k_{TF}^2} - \frac{1}{(k_1 + k_2)^2 + k_{TF}^2} \right) - \frac{2\pi k_{TF}^2}{3k_1 k_2} \left(\frac{1}{((k_1 - k_2)^2 + k_{TF}^2)^2} - \frac{1}{((k_1 + k_2)^2 + k_{TF}^2)^2} \right). \quad (\text{S.74})$$

Under the integration in Eq. (S.71), only the $(lm) = (00)$ term in Eq. (S.72) remains finite;

$$S_1 = \left(\prod_{i=1}^2 \int_0^{+\infty} \frac{dk_i}{(2\pi)^3} \right) k_i^2 f_{10}(\omega; k_1) c(k_1, k_2) f_{10}(\omega; k_2), \quad (\text{S.75})$$

with

$$\begin{aligned} c(k_1, k_2) &= \left(\theta(k_1 - K_{F,a}) \frac{-1}{2m_b} + \theta(K_{F,b} - k_1) \frac{1}{2m_a} \right) (2\pi)^3 \frac{\delta(k_1 - k_2)}{k_1^2} \\ &\quad + \beta_0(k_1, k_2) (4\pi) \left(\theta(k_1 - K_{F,a}) \theta(K_{F,b} - k_2) + \theta(k_2 - K_{F,a}) \theta(K_{F,b} - k_1) \right). \end{aligned} \quad (\text{S.76})$$

To numerically evaluate Eq. (S.75), we discretize k_1 and k_2 as in Eq. (S.34),

$$S_1 = \sum_{k_1, k_2} V_{10, k_1}^\omega C_{k_1 k_2} V_{10, k_2}^\omega, \quad (\text{S.77})$$

with

$$C_{k_1 k_2} \equiv \frac{k_1 k_2}{L(2\pi)^2} c(k_1, k_2) = \left(\theta(k_1 - K_{F,a}) \frac{-1}{2m_b} + \theta(K_{F,b} - k_1) \frac{1}{2m_a} \right) \delta_{k_1 k_2} + \frac{k_1 k_2}{L(2\pi)^2} \beta_0(k_1, k_2) (4\pi) \left(\theta(k_1 - K_{F,a}) \theta(K_{F,b} - k_2) + \theta(k_2 - K_{F,a}) \theta(K_{F,b} - k_1) \right). \quad (\text{S.78})$$

In summary, $b_j(\omega)$ is given by Eqs. (S.59, S.69, S.77) at $\omega = \pm\omega_{\pm}$. The energy-band curvatures of the lowest s -wave ($j = (100)$) exciton and antiexciton bands at the Γ point can be determined by $b_j(+\omega_+)$ and $b_j(-\omega_-)$ respectively;

$$\begin{cases} \xi_j(\mathbf{q}, \omega_+(\mathbf{q})) = (\omega_+(\mathbf{q}) - \omega_+) \left[\frac{d\xi_j(\mathbf{0}, \omega)}{d\omega} \right]_{|\omega=\omega_+} + b_j(\omega_+) q^2 = 0, & \text{for exciton,} \\ \xi_j(\mathbf{q}, -\omega_-(\mathbf{q})) = (-\omega_-(\mathbf{q}) + \omega_-) \left[\frac{d\xi_j(\mathbf{0}, \omega)}{d\omega} \right]_{|\omega=-\omega_-} + b_j(-\omega_-) q^2 = 0, & \text{for antiexciton.} \end{cases} \quad (\text{S.79})$$

From this, we obtain the energy-band curvatures of the exciton and antiexciton around the Γ point,

$$\begin{cases} \omega_+(\mathbf{q}) = \omega_+ - b_j(\omega_+) \left[\frac{d\xi_j(\mathbf{0}, \omega)}{d\omega} \right]_{|\omega=\omega_+}^{-1} q^2 + \dots, & \text{for exciton,} \\ \omega_-(\mathbf{q}) = \omega_- + b_j(-\omega_-) \left[\frac{d\xi_j(\mathbf{0}, \omega)}{d\omega} \right]_{|\omega=-\omega_-}^{-1} q^2 + \dots, & \text{for antiexciton.} \end{cases} \quad (\text{S.80})$$

- In 2D, $j = (nm)$. Take $(nm) = (10)$ and $\mathbf{e}_i = \mathbf{e}_x$. Since $\xi_j(\mathbf{0}, \pm\omega_{\pm}) = 0$, F_2 in Eq. (S.59) is given by

$$F_2 = - \sum_{nm \neq 10} \sum_{\mathbf{k}_1, \mathbf{k}_2, \mathbf{k}_3, \mathbf{k}_4} \frac{\langle \phi_{10}(\mathbf{0}, \omega) | \mathbf{k}_1 \rangle [\mathbf{F}_x]_{\mathbf{k}_1 \mathbf{k}_2} \langle \mathbf{k}_2 | \phi_{nm}(\mathbf{0}, \omega) \rangle \langle \phi_{nm}(\mathbf{0}, \omega) | \mathbf{k}_3 \rangle [\mathbf{F}_x]_{\mathbf{k}_3 \mathbf{k}_4} \langle \mathbf{k}_4 | \phi_{10}(\mathbf{0}, \omega) \rangle}{\xi_{nm}(\mathbf{0}, \omega)}. \quad (\text{S.81})$$

In terms of Eq. (S.48), we evaluate the matrix elements in F_2 by the 2D momentum integrals;

$$\sum_{\mathbf{k}_1, \mathbf{k}_2} \langle \phi_{10}(\mathbf{0}, \omega) | \mathbf{k}_1 \rangle [\mathbf{F}_x]_{\mathbf{k}_1 \mathbf{k}_2} \langle \mathbf{k}_2 | \phi_{nm}(\mathbf{0}, \omega) \rangle = \left(\prod_{i=1}^2 \int_0^{+\infty} \frac{k_i dk_i}{2\pi} \int_0^{2\pi} \frac{d\varphi_i}{2\pi} \right) f_{10}(\omega; k_1) \Omega \mathbf{F}_x(\mathbf{k}_1, \mathbf{k}_2) f_{nm}(\omega; k_2) e^{im\varphi_2}. \quad (\text{S.82})$$

Eq. (S.54) is decomposed in terms of the trigonometric functions,

$$\frac{2\pi}{(|\mathbf{k}_1 - \mathbf{k}_2| + k_{TF})^2} \frac{1}{|\mathbf{k}_1 - \mathbf{k}_2|} = \sum_m J_m(k_1, k_2) e^{im(\varphi_1 - \varphi_2)},$$

with

$$J_m(k_1, k_2) = \int_0^{2\pi} \frac{d(\varphi_1 - \varphi_2)}{2\pi} e^{-im(\varphi_1 - \varphi_2)} \frac{2\pi}{(\sqrt{k_1^2 + k_2^2 - 2k_1 k_2 \cos(\varphi_1 - \varphi_2)} + k_{TF})^2} \frac{1}{\sqrt{k_1^2 + k_2^2 - 2k_1 k_2 \cos(\varphi_1 - \varphi_2)}}. \quad (\text{S.83})$$

Eq. (S.81) is calculated in terms of the expansion,

$$\begin{aligned} & \langle \phi_{10}(\mathbf{0}, \omega) | \mathbf{F}_x | \phi_{nm}(\mathbf{0}, \omega) \rangle = \\ & \left(\prod_{i=1}^2 \int_0^{+\infty} \frac{dk_i}{2\pi} k_i \int_0^{2\pi} \frac{d\varphi_i}{2\pi} \right) f_{10}(\omega; k_1) f_{nm}(\omega; k_2) e^{im\varphi_2} \left\{ \right. \\ & \quad \theta(k_1 - K_{F,a}) \frac{k_1 (e^{i\varphi_1} + e^{-i\varphi_1})}{2m_b} \frac{2\pi \delta(k_1 - k_2)}{k_1} \sum_{m'} e^{im'(\varphi_1 - \varphi_2)} \\ & \quad + \theta(K_{F,b} - k_1) \frac{k_1 (e^{i\varphi_1} + e^{-i\varphi_1})}{2m_a} \frac{2\pi \delta(k_1 - k_2)}{k_1} \sum_{m'} e^{im'(\varphi_1 - \varphi_2)} \\ & \quad + \theta(k_1 - K_{F,a}) \theta(K_{F,b} - k_2) \left(\frac{k_1 (e^{i\varphi_1} + e^{-i\varphi_1})}{2} - \frac{k_2 (e^{i\varphi_2} + e^{-i\varphi_2})}{2} \right) \sum_{m'} J_{m'}(k_1, k_2) e^{im'\varphi_1} e^{-im'\varphi_2} \\ & \quad \left. + \theta(k_2 - K_{F,a}) \theta(K_{F,b} - k_1) \left(\frac{k_2 (e^{i\varphi_2} + e^{-i\varphi_2})}{2} - \frac{k_1 (e^{i\varphi_1} + e^{-i\varphi_1})}{2} \right) \sum_{m'} J_{m'}(k_1, k_2) e^{im'\varphi_1} e^{-im'\varphi_2} \right\}. \quad (\text{S.84}) \end{aligned}$$

Under the momentum integration, only $m = \pm 1$ terms remain finite in Eq. (S.82). Since $f_{nm}(\omega; k) = f_{n(-m)}(\omega; k)$, $\xi_{nm}(\omega; k) = \xi_{n(-m)}(\omega; k)$, and $J_m(k, k') = J_{-m}(k, k')$, the matrix elements for $m = +1$ and those for $m = -1$ are the same,

$$\langle \phi_{10}(\mathbf{0}, \omega) | \mathbf{F}_x | \phi_{n(\pm 1)}(\mathbf{0}, \omega) \rangle = \left(\prod_{i=1}^2 \int_0^{+\infty} \frac{dk_i}{2\pi} \quad k_i \right) f_{10}(\omega; k_1) \tau(k_1, k_2) f_{n1}(\omega; k_2), \quad (\text{S.85})$$

with

$$\begin{aligned} \tau(k_1, k_2) &= \theta(k_1 - K_{F,a}) \frac{2\pi\delta(k_1 - k_2)}{2m_b} + \theta(K_{F,b} - k_1) \frac{2\pi\delta(k_1 - k_2)}{2m_a} \\ &+ \theta(k_1 - K_{F,a}) \theta(K_{F,b} - k_2) \left(\frac{k_1}{2} J_1(k_1, k_2) - \frac{k_2}{2} J_0(k_1, k_2) \right) \\ &+ \theta(k_2 - K_{F,a}) \theta(K_{F,b} - k_1) \left(\frac{k_2}{2} J_0(k_1, k_2) - \frac{k_1}{2} J_1(k_1, k_2) \right). \end{aligned} \quad (\text{S.86})$$

Then we finally have

$$F_2 = -2 \left(\prod_{i=1}^4 \int_0^{+\infty} \frac{dk_i}{2\pi} \quad k_i \right) \sum_n \frac{1}{\xi_{n1}(\mathbf{0}, \omega)} f_{10}(\omega; k_1) \tau(k_1, k_2) f_{n1}(\omega; k_2) f_{n1}(\omega; k_3) \tau(k_3, k_4) f_{10}(\omega; k_4). \quad (\text{S.87})$$

To evaluate Eq. (S.87) numerically, we discretize k_i ($i = 1, 2, 3, 4$) as in Eq. (S.34),

$$F_2 = -2 \sum_{k_1, k_2, k_3, k_4} \sum_n V_{10, k_1}^\omega T_{k_1 k_2} V_{n1, k_2}^\omega \frac{1}{\xi_{n1}(\mathbf{0}, \omega)} V_{n1, k_3}^\omega T_{k_3 k_4} V_{10, k_4}^\omega = -2 \sum_{k_1, k_2, k_3, k_4} V_{10, k_1}^\omega T_{k_1 k_2} H_{1, k_2 k_3}^{\omega, -1} T_{k_3 k_4} V_{10, k_4}^\omega. \quad (\text{S.88})$$

Here $V_{nm, k}^\omega$ and $H_{m, k k'}^\omega$ are defined in Eq. (S.45) and

$$\begin{aligned} T_{k_1 k_2} &\equiv \frac{\sqrt{k_1 k_2}}{L} \tau(k_1, k_2) = \left(\theta(k_1 - K_{F,a}) \frac{k_1}{2m_b} + \theta(K_{F,b} - k_1) \frac{k_1}{2m_a} \right) \delta_{k_1 k_2} \\ &+ \frac{\sqrt{k_1 k_2}}{L} \left\{ \theta(k_1 - K_{F,a}) \theta(K_{F,b} - k_2) \left(\frac{k_1}{2} J_1(k_1, k_2) - \frac{k_2}{2} J_0(k_1, k_2) \right) \right. \\ &\left. + \theta(k_2 - K_{F,a}) \theta(K_{F,b} - k_1) \left(\frac{k_2}{2} J_0(k_1, k_2) - \frac{k_1}{2} J_1(k_1, k_2) \right) \right\}. \end{aligned} \quad (\text{S.89})$$

S_1 in Eq. (S.59) is given by the 2D momentum integrals,

$$\begin{aligned} S_1 &= \sum_{\mathbf{k}_1, \mathbf{k}_2} \langle \phi_{10}(\mathbf{0}, \omega) | \mathbf{k}_1 \rangle [\mathbf{S}_x]_{\mathbf{k}_1, \mathbf{k}_2} \langle \mathbf{k}_2 | \phi_{10}(\mathbf{0}, \omega) \rangle = \frac{1}{2} \sum_{\mathbf{k}_1, \mathbf{k}_2} \langle \phi_{10}(\mathbf{0}, \omega) | \mathbf{k}_1 \rangle [\mathbf{S}_x + \mathbf{S}_y]_{\mathbf{k}_1, \mathbf{k}_2} \langle \mathbf{k}_2 | \phi_{10}(\mathbf{0}, \omega) \rangle \\ &= \left(\prod_{i=1}^2 \int_0^{+\infty} \frac{dk_i}{2\pi} \quad k_i \int_0^{2\pi} \frac{d\varphi_i}{2\pi} \right) f_{10}(\omega; k_1) \Omega \mathbf{S}(\mathbf{k}_1, \mathbf{k}_2) f_{10}(\omega; k_2). \end{aligned} \quad (\text{S.90})$$

$\Omega \mathbf{S} = \frac{\Omega}{2} (\mathbf{S}_x + \mathbf{S}_y)$ is further expanded in terms of the Fourier series,

$$\begin{aligned} \Omega \mathbf{S}(\mathbf{k}_1, \mathbf{k}_2) &= \left(\theta(k_1 - K_{F,a}) \frac{-1}{2m_b} + \theta(K_{F,b} - k_1) \frac{1}{2m_a} \right) \frac{2\pi\delta(k_1 - k_2)}{k_1} \sum_m e^{im(\varphi_1 - \varphi_2)} \\ &+ \left(\theta(k_1 - K_{F,a}) \theta(K_{F,b} - k_2) + \theta(k_2 - K_{F,a}) \theta(K_{F,b} - k_1) \right) \sum_m K_m(k_1, k_2) e^{im(\varphi_1 - \varphi_2)}, \end{aligned} \quad (\text{S.91})$$

with Fourier coefficients

$$\begin{aligned} K_m(k_1, k_2) &= \frac{1}{2} \int_0^{2\pi} \frac{d(\varphi_1 - \varphi_2)}{2\pi} e^{-im(\varphi_1 - \varphi_2)} \left\{ \frac{2\pi}{(\sqrt{k_1^2 + k_2^2} - 2k_1 k_2 \cos(\varphi_1 - \varphi_2) + k_{TF})^3} \right. \\ &\left. - \frac{\pi}{(\sqrt{k_1^2 + k_2^2} - 2k_1 k_2 \cos(\varphi_1 - \varphi_2) + k_{TF})^2} \frac{1}{\sqrt{k_1^2 + k_2^2 - 2k_1 k_2 \cos(\varphi_1 - \varphi_2)}} \right\}. \end{aligned} \quad (\text{S.92})$$

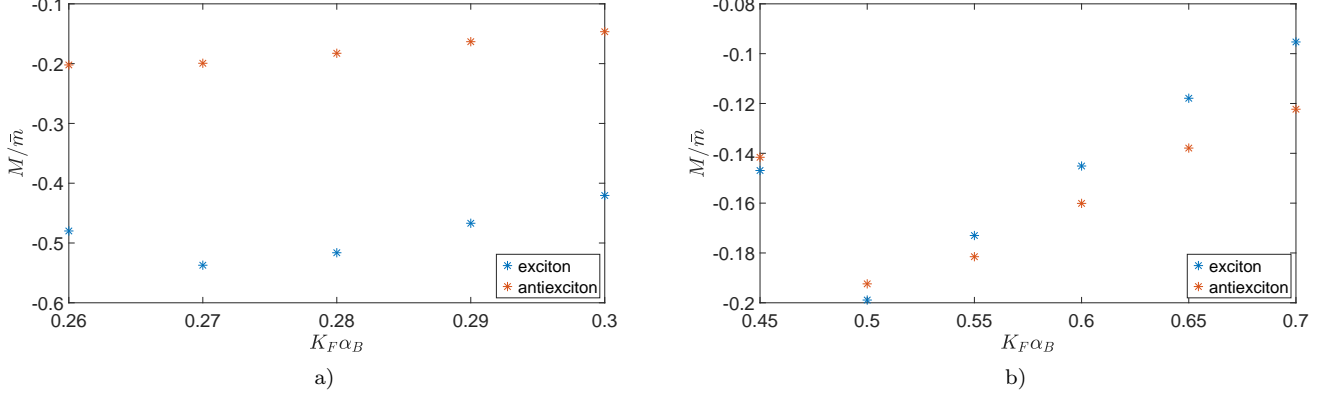


FIG. S.4. Ratios between masses of the s -wave exciton and antiexciton bands and the mass of the electron and hole bands $\tilde{m} \equiv m_a = m_b$. The Ratios are plotted as a function of a dimensionless quantity $K_F\alpha_B$, where $K_F \equiv (K_{F,a} + K_{F,b})/2$ and $\alpha_B \equiv 1/\tilde{m}$ (the effective Bohr radius of the electron system). The exciton's and antiexciton's masses are defined in the expansion $\omega_{\pm}(\mathbf{q})$ around the Γ point, $\omega_{\pm}(\mathbf{q}) \equiv \omega_{\pm} + q^2/(2M)$. (a) The 3D case. (b) The 2D case. In these two plots, we choose $\tilde{E}_g = -1.03$ and $\tilde{\mu} = 0.172$, which are the same value as we take in Fig. 3 and Fig. 4 in the main text.

Under the integrals over φ_1 and φ_2 in Eq. (S.90), only $m = 0$ term in Eq. (S.91) remains finite,

$$S_1 = \left(\prod_{i=1}^2 \int_0^{+\infty} \frac{dk_i}{2\pi} k_i \right) f_{10}(\omega; k_1) \chi(k_1, k_2) f_{10}(\omega; k_2), \quad (\text{S.93})$$

with

$$\begin{aligned} \chi(k_1, k_2) = & \left(\theta(k_1 - K_{F,a}) \frac{-1}{2m_b} + \theta(K_{F,b} - k_1) \frac{1}{2m_a} \right) \frac{2\pi\delta(k_1 - k_2)}{k_1} \\ & + \left(\theta(k_1 - K_{F,a})\theta(K_{F,b} - k_2) + \theta(k_2 - K_{F,a})\theta(K_{F,b} - k_1) \right) K_0(k_1, k_2). \end{aligned} \quad (\text{S.94})$$

To evaluate Eq. (S.93) numerically, we put it in a discrete form

$$S_1 = \sum_{k_1, k_2} V_{10, k_1}^{\omega} X_{k_1 k_2} V_{10, k_2}^{\omega}, \quad (\text{S.95})$$

where $V_{nm, k}^{\omega}$ are defined in Eq. (S.45) and

$$\begin{aligned} X_{k_1 k_2} = & \frac{\sqrt{k_1 k_2}}{L} \chi(k_1, k_2) = \left(\theta(k_1 - K_{F,a}) \frac{-1}{2m_b} + \theta(K_{F,b} - k_1) \frac{1}{2m_a} \right) \delta_{k_1 k_2} \\ & + \frac{\sqrt{k_1 k_2}}{L} \left(\theta(k_1 - K_{F,a})\theta(K_{F,b} - k_2) + \theta(k_2 - K_{F,a})\theta(K_{F,b} - k_1) \right) K_0(k_1, k_2). \end{aligned} \quad (\text{S.96})$$

In summary, $b_j(\omega)$ is given by Eqs. (S.59, S.88, S.95) evaluated at $\omega = \pm\omega_{\pm}$. The energy-band curvatures of exciton and antiexciton bands are obtained by Eqs. (S.79, S.80).

We can see from the expression in Eq. (S.59) that the F_2 term is always positive. Our numerical calculation shows that in parameter regions we studied, F_2 term dominates over the S_1 term, which makes $b_j(\omega_+)$ and $b_j(-\omega_-)$ to be always positive. Thus, from Eq. (S.80), we can see that the band curvatures around the Γ point become negative. In Fig. S.4, we show the values of the band curvatures as we vary the electron mass \tilde{m} ($m_a = m_b$) and fix E_g and μ .

Possible annihilation processes of an exciton-antiexciton pair

The main text discusses possible annihilation processes of an exciton-antiexciton pair into multiple intra-band collective excitations or individual excitations. The process is constrained by the momentum and energy conservation,

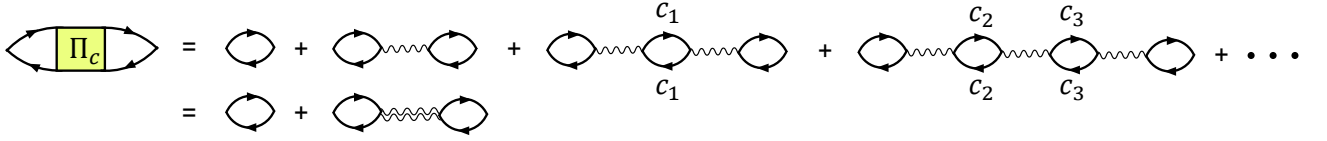


FIG. S.5. Feynman diagrams of the RPA contributions to the polarization function $\Pi^c(\mathbf{q}, \omega)$ ($c = a$ or b). The single- and double-wavy lines represent bare (long-ranged) and screened Coulomb interactions, respectively. Solid lines without labels correspond to the free single-particle Green's function of the c band. Solid lines with labels c_j stand for the free single-particle Green's functions of the c_j band ($c_j = a, b$). The summation over c_1, c_2, c_3 and \dots are implicit in the right-hand side.

where momentum-energy dispersions of the inter-band/intra-band collective/individual excitations are relevant. In this section, we show the momentum-energy dispersions of intra-band and inter-band collective excitations around the Γ point for a specific set of parameters with $m_a = m_b = \bar{m}$, $\mu > 0$, and $K_{F,a} > K_{F,b}$.

Due to the presence of the Fermi surfaces, individual excitations form continuum spectra on the $\omega - q$ plane. Borders of the continuum spectra for the intra-band individual excitations for the a and b bands are given by $(q^2 \pm 2K_{F,a}q)/(2m)$ and $(q^2 \pm 2K_{F,b}q)/(2m)$, respectively [30]. Intra-band density-wave modes form momentum-energy dispersions outside the continuum spectra. The dispersion of the intra-band density modes can be calculated from the polarization functions of the a -band and b -band densities, $\Pi_c(\mathbf{x} - \mathbf{x}', t - t') = -i\langle 0 | \mathcal{T} \{ [\hat{\rho}^c(\mathbf{x}, t) - \rho_0^c] [\hat{\rho}^c(\mathbf{x}', t') - \rho_0^c] \} | 0 \rangle$. Here $\hat{\rho}^c$ and ρ_0^c represent the c -band density operator and its ground-state average, respectively ($c = a, b$). Let $\Pi_c(\mathbf{q}, \omega)$ be the Fourier transform of $\Pi_c(\mathbf{x} - \mathbf{x}', t - t')$.

In terms of random phase approximation (RPA), $\Pi^c(\mathbf{q}, \omega)$ is calculated as follows (Fig. S.5):

$$\begin{aligned} \Pi^c(\mathbf{q}, \omega) &= \Pi_0^c(\mathbf{q}, \omega) + \Pi_0^c(\mathbf{q}, \omega) w(\mathbf{q}, \omega) \Pi_0^c(\mathbf{q}, \omega) \\ &= \Pi_0^c(\mathbf{q}, \omega) \frac{1 - [\Pi_0(\mathbf{q}, \omega) - \Pi_0^c(\mathbf{q}, \omega)] v(\mathbf{q})}{1 - \Pi_0(\mathbf{q}, \omega) v(\mathbf{q})}, \end{aligned} \quad (\text{S.97})$$

where $\Pi_0^c(\mathbf{q}, \omega)$ and $\Pi_0(\mathbf{q}, \omega)$ are given by Eq. (S.13). Thus, the intra-band density-wave modes for the two bands share the same denominator and the zeros of the denominator determine the momentum-energy dispersions of the plasmon mode,

$$1 - \Pi_0(\mathbf{q}, \omega) v(\mathbf{q}) = 0. \quad (\text{S.98})$$

Using the Lindhard function at the limit of $q \rightarrow 0$ for 3D and $q \rightarrow 0, \omega \rightarrow 0$ for 2D [18, 22, 30],

$$\Pi_0^c(q, \omega) = \begin{cases} -\frac{m_c K_{F,c}}{4\pi^2} \left(2 - x_c \ln \left(\frac{x_c + 1}{x_c - 1} \right) \right) & \text{in 3D,} \\ -\frac{m_c}{2\pi} \left(1 - \frac{x_c}{\sqrt{x_c^2 - 1}} \right) & \text{in 2D,} \end{cases} \quad (\text{S.99})$$

with $x_c \equiv \frac{m_c \omega}{K_{F,c} q}$ ($c = a, b$), we further take $\omega \gg q$ and expand $\Pi_0(\mathbf{q}, \omega) \equiv \Pi_0^a(q, \omega) + \Pi_0^b(q, \omega)$ up to the fourth order of $\frac{1}{x_a}$ and $\frac{1}{x_b}$. Then we solve Eq. (S.98) in favor of ω up to the subleading order in small q . This gives out

$$\omega = \begin{cases} \sqrt{A_3} \left(1 + \frac{B_3}{2A_3^2} q^2 \right) & \text{in 3D,} \\ \sqrt{A_2} q \left(1 + \frac{B_2}{2A_2^2} q \right) & \text{in 2D,} \end{cases} \quad (\text{S.100})$$

$$\text{with } A_3 = \sum_{c=a,b} \frac{2K_{F,c}^2}{3\pi m_c}, \quad B_3 = \sum_{c=a,b} \frac{2K_{F,c}^5}{5\pi m_c^3}, \quad A_2 = \sum_{c=a,b} \frac{K_{F,c}^2}{2m_c}, \quad B_2 = \sum_{c=a,b} \frac{3K_{F,c}^4}{8m_c^3}.$$

Fig. S.6 shows a region of the continuum spectra of the intra-band individual excitations, the dispersions of the plasmon modes, and momentum-energy dispersions of the s -wave exciton and antiexciton bands. The band dispersions for the exciton and antiexciton bands are calculated only around the Γ point by Eqs. (S.80). The figure shows that the plasmon oscillation in the 3D case appears at much higher energies than the exciton and antiexciton bands. Thereby, it is likely that the exciton-antiexciton pair in the 3D case only decays into intra-band individual excitations. In the 2D case, the plasmon dispersion is gapless, where an exciton-antiexciton pair decays either into intra-band individual excitations or into density-wave modes.

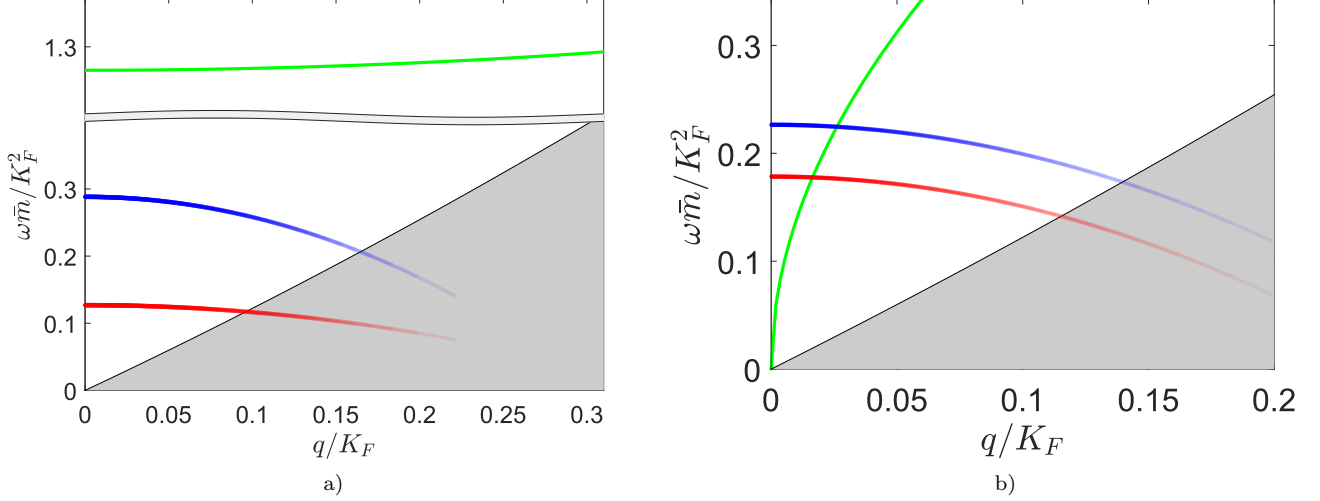


FIG. S.6. Energy-momentum dispersions of the s -wave exciton and antiexciton bands (the red and blue lines), plasmon bands (the green lines) and continuum spectra of the intra-band individual excitations (the grey shaded regions). The dispersions for $\tilde{m} = m_a = m_b$ are determined by three dimensionless quantities, $K_F \alpha_B$, $\tilde{E}_g \equiv E_g \tilde{m} / K_F^2$ and $\tilde{\mu} \equiv \mu \tilde{m} / K_F^2$, where $K_F \equiv (K_{F,a} + K_{F,b})/2$ and the effective Bohr radius $\alpha_B \equiv 1/\tilde{m}$. (a) The 3D case with $K_F \alpha_B = 0.289$, $\tilde{E}_g = -1.03$, and $\tilde{\mu} = 0.172$. (b) The 2D case with $K_F \alpha_B = 0.540$, $\tilde{E}_g = -1.03$, and $\tilde{\mu} = 0.172$. The quantum numbers of the s -wave exciton and antiexciton are $(nlm) = (100)$ in the 3D case and $(nm) = (10)$ in the 2D case (see the text).

Conserved-charge analyses of the effective field theory

From Noether's theorem, the effective Lagrangian of Eq. (11) in the main text has the conserved charge density [1]

$$j^0 = -i\varphi \frac{\partial \mathcal{L}}{\partial(\partial_t \varphi)} + i\varphi^\dagger \frac{\partial \mathcal{L}}{\partial(\partial_t \varphi^\dagger)} = i\gamma [\varphi^\dagger (\partial_t \varphi) - (\partial_t \varphi^\dagger) \varphi] + \alpha \varphi^\dagger \varphi. \quad (\text{S.101})$$

From Eq. (14) in the main text, φ is given by a linear combination of the annihilation of the exciton (a_+) and the creation of the antiexciton (a_-^\dagger);

$$\varphi = \frac{1}{\sqrt{\lambda\eta}} (a_+ + a_-^\dagger). \quad (\text{S.102})$$

a_+ and a_- have their dynamical evolutions in the interaction picture for a quantum-mechanical problem; $a_+(t) = a_+ e^{-i\nu_+ t}$, $a_-(t) = a_- e^{-i\nu_- t}$. From Eqs. (S.101, S.102) together with the time evolutions, one can readily see that the density is time-independent and is given by the difference between the exciton and antiexciton density;

$$\begin{aligned} j^0(t) &= \frac{\gamma}{\lambda\eta} \left[(a_+^\dagger e^{i\nu_+ t} + a_- e^{-i\nu_- t}) (\nu_+ a_+ e^{-i\nu_+ t} - \nu_- a_-^\dagger e^{i\nu_- t}) + \text{h.c.} \right] + \frac{\alpha}{\lambda\eta} (a_+^\dagger e^{i\nu_+ t} + a_- e^{-i\nu_- t}) (a_+ e^{-i\nu_+ t} + a_-^\dagger e^{i\nu_- t}) \\ &= \frac{\alpha + 2\gamma\nu_+}{\lambda\eta} a_+^\dagger a_+ + \frac{\alpha - 2\gamma\nu_-}{\lambda\eta} a_-^\dagger a_- + \frac{\gamma(\nu_+ - \nu_-) + \alpha}{\lambda\eta} [a_+^\dagger a_-^\dagger e^{i(\nu_+ + \nu_-)t} + \text{h.c.}] \\ &= a_+^\dagger a_+ - a_-^\dagger a_-. \end{aligned} \quad (\text{S.103})$$

Here $\nu_\pm = \eta \mp \alpha/(2\gamma)$ and $\lambda = 2\gamma$. Thus, the particle a_+ carries charge +1, while the antiparticle a_- carries charge -1.